POLITECNICO DI TORINO
Repository ISTITUZIONALE

Integrating Satellite Data Into Meso-Scale Habitat Modeling for Non-Perennial Rivers and Streams

Original
Integrating Satellite Data Into Meso-Scale Habitat Modeling for Non-Perennial Rivers and Streams / Negro, G., Pinna, B., Manfreda, G., Lo Conte, P., Belcore, E., Maschio, P., Cavallo, C., Papa, M.N., Vezza, P.. - In: WATER RESOURCES RESEARCH. - ISSN 0043-1397. - 62:3(2026). [10.1029/2025WR041133]

Availability:
This version is available at: 11583/3016506 since: 2026-10-10T15:26:15Z

Publisher:
Wiley

Published
DOI:10.1029/2025WR041133

Terms of use:

This article is made available under terms and conditions as specified in the corresponding bibliographic description in the repository

Publisher copyright

(Article begins on next page)

13 November 2026

Check for updates

Water Resources Research

RESEARCH ARTICLE
10.1029/2025WR041133

Integrating Satellite Data Into Meso-Scale Habitat Modeling for Non-Perennial Rivers and Streams

G. Negro[1], B. Pinna[1], G. Manfreda[1], P. Lo Conte[2], E. Belcore[1], P. Maschio[1], C. Cavallo[3], M. N. Papa[3], and P. Vezza[1]

[1]Department of Environment, Land and Infrastructure Engineering, Polytechnic of Turin, Torino, Italy, [2]Funzione specializzata Tutela Fauna e Flora, Torino, Italy, [3]Department of Civil Engineering, University of Salerno, Fisciano, Italy

Key Points:

- Habitat availability in non-perennial rivers can be assessed for both fish and macroinvertebrates
- Satellite imagery enables a clear description of flow intermittency, estimating the duration of the flowing, ponding and dry conditions
- The new MesoHABSIM module for non-perennial rivers accurately models aquatic habitat dynamics during both flowing and non-flowing phases

Supporting Information:

Supporting Information may be found in the online version of this article.

Correspondence to:

G. Negro,
giovanni.negro@polito.it

Citation:

Negro, G., Pinna, B., Manfreda, G., Lo Conte, P., Belcore, E., Maschio, P., et al. (2026). Integrating satellite data into meso-scale habitat modeling for non-perennial rivers and streams. *Water Resources Research*, *62*, e2025WR041133. https://doi.org/10.1029/2025WR041133

Received 22 MAY 2025
Accepted 20 FEB 2026

Author Contributions:

Conceptualization: G. Negro, C. Cavallo, M. N. Papa, P. Vezza
Investigation: G. Negro
Methodology: G. Negro, B. Pinna, G. Manfreda, P. Lo Conte, E. Belcore, P. Maschio, C. Cavallo, M. N. Papa, P. Vezza
Supervision: P. Vezza
Writing – original draft: G. Negro
Writing – review & editing: B. Pinna, G. Manfreda, P. Lo Conte, E. Belcore, C. Cavallo, M. N. Papa, P. Vezza

© 2026. The Author(s).
This is an open access article under the terms of the Creative Commons Attribution License, which permits use, distribution and reproduction in any medium, provided the original work is properly cited.

Abstract Non-perennial rivers and streams (NPRs) are widespread and projected to become more common, yet effective tools for their characterization and management remain limited. This study introduces a novel approach to assess aquatic habitat availability in NPRs, applied to a regulated reach of the Sangone River (Northern Italy). Using the NPRs-module of the MesoHABitat Simulation Model (MesoHABSIM), we evaluated habitat dynamics for two native fish species (*Telestes muticellus* and *Padogobius bonelli*) and the macroinvertebrate community (Flow-T index), in relation to streamflow and the time elapsed since discharge cessation. Habitat characterization was supported by high-resolution geospatial and field data collected in July 2021. To analyze flow intermittency, over 1700 multisource satellite images (monitoring period: 2017–2023) were classified in flowing, ponding, and dry conditions. This information, combined with local hydrological data, enabled the estimation of ponding durations (median = 8 days), a key factor for evaluating aquatic habitat persistence during non-flowing phases, and identification of the driest period (i.e., summer 2022), warranting focused habitat analysis. Habitat availability varied across ecological targets: adult *T. muticellus* preferred higher flows (>1 m^3/s) and suffered rapid habitat loss during ponding, making it highly vulnerable to intermittency. In contrast, juveniles and *P. bonelli* favored lower flows (~0.15 m^3/s) and declined more gradually after flow interruption. For macroinvertebrates, suitable habitat increased monotonically with flow and showed the highest persistence during the ponding condition. This study provides an effective methodology for NPR characterization and aquatic habitat analysis, offering insights to guide ecological flow strategies to support NPRs ecosystem conservation.

1. Introduction

Non-perennial rivers and streams (NPRs, Busch et al., 2020) are generally defined as streams that experience a lack of surface flow during some portion of the year (McDonough et al., 2011). According to the occurrence and duration of the zero-flow conditions, they can be distinguished into intermittent rivers or episodic/ephemeral streams (Arthington et al., 2014). The former rarely achieve a waterless status, the latter frequently experience the disappearance of the surface water (Anna et al., 2009). Laid on the borderline between aquatic and terrestrial ecosystems, NPRs continuously shift their status according to the fluctuation of their hydrological condition, which modifies the nature of their ecosystems from lotic to lentic until a terrestrial one (Datry et al., 2017). Gallart et al. (2017) identified three primary hydrological conditions that essentially characterized NPRs: flowing (F), ponding (P), and dry (D) conditions, with P and D conditions collectively referred to as the non-flowing (NF) phase. The F condition indicates a continuous surface flow within the river channel. In contrast, the P condition is defined by the presence of water within the river channel organized in patches of disconnected wetted areas (e.g., isolated ponds), when surface flow is equal or very close to zero. Lastly, the D condition implies the absence of surface water.

Recent studies suggest that NPRs are likely the most widespread type of rivers on Earth (Messager et al., 2021), comprising more than half of the global river network (Datry et al., 2017). These watercourses dominate arid and semi-arid regions (Larned et al., 2010), and are especially prevalent in Mediterranean watersheds, where the marked dry/wet climate patterns favor their occurrence (McDonough et al., 2011; Tzoraki & Nikolaidis, 2007). However, flow intermittency is projected to expand globally in future scenarios due to various anthropogenic pressures, including climate change and increasing water withdrawals (e.g., Döll & Schmied, 2012; Pumo et al., 2016; Sauquet et al., 2021). Over recent decades, major rivers such as the Nile, Yellow, Indus, and Colorado, previously known for being perennial, have experienced NF conditions in some reaches (Datry et al., 2014).

19447973, 2026, 3, Downloaded from https://agupubs.onlinelibrary.wiley.com/doi/10.1029/2025WR041133 by Politecnico Di Torino Sist. Bibl Del Polit Di Torino, Wiley Online Library on [07/10/2026]. See the Terms and Conditions (https://onlinelibrary.wiley.com/terms-and-conditions) on Wiley Online Library for rules of use; OA articles are governed by the applicable Creative Commons License

NPRs provide essential ecosystem services (Yeakley et al., 2016), including groundwater recharge, flood regulation, sediment transport, and habitat connectivity (Magand et al., 2020). They also support biogeochemical processes and biodiversity, particularly in Mediterranean regions where they sustain numerous unique and endemic freshwater species, many of which are currently threatened or endangered (Skoulikidis et al., 2017). Despite their ecological significance and widespread distribution, NPRs often suffer from low public and institutional recognition. They have historically been undervalued, perceived as less ecologically and economically important than perennial rivers (Larned et al., 2010; Llanos-Paez & Acuña, 2022).

Regulatory frameworks have also contributed to the marginalization of NPRs. In Europe, the Water Frame Directive (WFD, European Union, 2000), although intended to protect all freshwater bodies, effectively excludes a significant number of non-perennial streams from biomonitoring primarily due to their typically small catchment areas (<10 km^2). Furthermore, assessing the ecological status of NPRs is often neglected or deemed impractical, as current evaluation methods rely heavily on indices originally developed for perennial rivers (Munné et al., 2021). This exclusion highlights a gap in regulatory frameworks, which hinders effective management practices crucial for preserving NPR ecosystems and the services they provide (Leone et al., 2023). Effective environmental management of NPRs is also precluded by the lack of a robust hydrological monitoring network, resulting in a scarcity of flow data and limited understanding of the occurrence of NF periods within river networks. Traditional monitoring networks rely predominantly on in situ measurements (e.g., stream gauging stations or observation wells), which are generally sparse, especially within NPR reaches (Messager et al., 2021), and often lack continuous, long-term data sets (Krabbenhoft et al., 2022). Moreover, gauging stations provide only point-based data that fail to capture the spatio-temporal complexity of flow intermittency (Cavallo et al., 2022). Even when zero flow is recorded, this does not necessarily imply a completely dry riverbed (Zimmer et al., 2020), as isolated wetted areas may persist after flow cessation (Bonada et al., 2020). Similarly, groundwater-level data from observation wells offer limited utility for characterizing NPR hydrology, as the distinction between P and D conditions is often unclear. Indeed, the persistence of surface water after flow cessation may result from a variety of hydrological and geomorphological mechanisms that are not directly linked to local groundwater levels (Bourke et al., 2021). Finally, the sparse and fragmented nature of monitoring networks restricts the calibration and validation of hydrological models (e.g., rainfall-runoff models), thereby limiting their ability to accurately simulate flow variability in NPRs (Gallart et al., 2017).

Recent advancements in remote sensing technologies provide new opportunities to address these gaps, promoting pioneering studies to monitor flow intermittency in river networks using satellite data (Maswanganye et al., 2022). These approaches have demonstrated potential for characterizing NPR regimes, as they enable efficient monitoring of large areas with high temporal resolution in a cost-effective manner. Among the available optical satellite constellations, the Sentinel-2 (S2) and PlanetScope (PS) have proven particularly effective, offering an optimal balance between Ground Sample Distance (GSD) and revisit time. For instance, Cavallo et al. (2022) proposed a supervised classification approach using freely available S2 false-color images (FCIs) to identify NPRs and assess their temporariness based on the duration of local hydrological conditions. In another study, Cavallo et al. (2025), using Sentinel-2 imagery, developed an automatic approach to estimate the duration of the dry bed condition in a NPR of Southern Italy. Similarly, Maswanganye et al. (2024) used multispectral indices for assessing the hydrological conditions of NPRs by combining Sentinel-1 and Sentinel-2 data sets. Additionally, Tayer, Beesley, Douglas, Bourke, Callow, et al. (2023) utilized S2 imagery to derive ecohydrological metrics, describing wetted area attributes and their temporal changes in a large lowland intermittent river. In another study, Tayer, Beesley, Douglas, Bourke, Meredith, et al. (2023) applied clustering techniques to identify hydrological zones along a 400 km river reach, uncovering spatial patterns in water persistence and longitudinal connectivity. Focusing on PS imagery, Wang and Vivoni (2022) introduced an innovative method leveraging the near-infrared (NIR) band to detect flowing conditions in NPRs.

Despite these advancements concerning the hydrological characterization, dedicated approaches for defining appropriate ecological flows (e-flows, Bussettini & Vezza, 2019) in NPRs remain largely underrepresented (Leone et al., 2023). Traditional hydrological (e.g., Tennant, 1976) and holistic (e.g., Poff et al., 2010) methods, designed for perennial rivers, have proven unsuitable for NPRs, as they do not account for the natural intermittency of streamflow (Acuña et al., 2020). More recent studies, however, have demonstrated the potential of adapting both hydrological (e.g., Acuña et al., 2020; Dornes & Comas, 2025) and holistic approaches (e.g., Seaman et al., 2016) to NPR contexts. Habitat modeling approaches have also been rarely applied to define

19447973, 2026, 3, Downloaded from https://agupubs.onlinelibrary.wiley.com/doi/10.1029/2025WR041133 by Politecnico Di Torino Sist. Bibl Del Polit Di Torino, Wiley Online Library on [07/10/2026]. See the Terms and Conditions (https://onlinelibrary.wiley.com/terms-and-conditions) on Wiley Online Library for rules of use; OA articles are governed by the applicable Creative Commons License

e-flows in NPRs (Acuña et al., 2020). Major limitations of traditional micro-scale habitat suitability models (e.g., Bovee, 1982; Jorde, 1997) arise in assessing and describing the complex aquatic habitat dynamics when discharge approaches zero or when remaining aquatic habitats are represented by isolated, disconnected ponds (Acuña et al., 2020). After flow interruption, indeed, the water surface typically moves into a framing of isolated wetted areas that still potentially provide a suitable environment for freshwater species (McDonough et al., 2011). The habitat pattern during the P condition is clearly dependent on the local hydro-geomorphological features of the river (e.g., groundwater table, shape and planforms of the channel), but it is ultimately governed by the amount of time elapsed since discharge ceased (Acuña et al., 2020). To model habitat evolution during both F and NF phases, a new module was recently developed within the MesoHABitat SImulation Model (MesoHABSIM, Parasiewicz, 2007) specifically designed for analyzing NPRs (i.e., the NPRs-module, Acuña et al., 2020; Negro et al., 2019). This module was created to address key objectives: (a) designing e-flows to mitigate the impacts of river damming and water abstraction on freshwater ecosystems, (b) evaluating the effectiveness of river restoration projects, and (c) providing actionable insights to support freshwater species conservation programs in NPRs. By adopting a meso-scale perspective, the MesoHABSIM approach overcomes many limitations of traditional micro-scale habitat suitability models (e.g., Bovee, 1982). It employs mesohabitats, or Geomorphic Units (GUs; Belletti et al., 2017), as the primary spatial units of analysis, which are recognized as significant structural components of river systems, closely linked to the life cycles of various aquatic communities (Kemp et al., 1999; Petts, 2009). Compared to micro-scale models, MesoHABSIM offers a more comprehensive and ecologically realistic depiction of aquatic habitats, enabling a better representation of longitudinal habitat variability (Vezza, Parasiewicz, Spairani, & Comoglio, 2014), which is especially valuable for describing P conditions in NPRs. Moreover, meso-scale modeling integrates a wider range of ecologically relevant parameters, such as cover, refugia, and substrate types, which are critical for different aquatic communities (Parasiewicz, Ryan, et al., 2013; Wegscheider et al., 2020). Furthermore, MesoHABSIM effectively enables the integration of high-resolution spatial information, either collected using proximal sensing or derived from hydrodynamic simulations (e.g., Farò et al., 2022), to assess habitat availability for diverse freshwater organisms (e.g., Negro et al., 2023; Pinna et al., 2024).

This study introduces a novel approach to assess fish and macroinvertebrate habitat availability in NPRs during both F and NF phases by integrating advanced habitat modeling tools with remote sensing technologies. To model the evolution of aquatic habitat in relation to flow conditions and the time elapsed after flow cessation (NF phase), the innovative NPRs-module of the MesoHABSIM approach, integrated into the SimStream-Web service (Politecnico di Torino (DIATI), 2024), was employed. Physical habitat description was achieved using high-resolution aerial imagery acquired via Uncrewed Aerial Systems (UAS), complemented by two-dimensional (2D) hydrodynamic modeling and field measurements. Data from S2 and PS satellite missions, together with locally recorded hydrological data, were used to characterize the hydrological regime and quantify the duration of the P condition, prior to a completely dry riverbed, over a 7-year monitoring period (2017–2023). The outcomes of both analyses were integrated to analyze the spatio-temporal variability of aquatic habitat availability in a regulated, hydro-morphologically homogeneous reach of the Sangone River (Northern Italy).

2. Materials and Methods

2.1. Study Area

To apply meso-scale habitat modeling to NPRs, a regulated hydro-morphologically homogeneous reach of the Sangone River was used as a case study. The Sangone is a small stream that entirely flows within the Piemonte Region (Northern Italy, Figure 1). Originating from the Alps at an elevation of 2,000 m above sea level, it stretches for nearly 50 km until it joins the Po River near the metropolitan city of Torino, situated at 220 m above sea level. The river's average slope is 2.7%, and its catchment area covers 268 km^2, occupied almost equally by plains (53%) and mountainous areas (47%).

The Sangone catchment can be divided into two main parts, delineated by a noticeable narrowing of its basin near the village of Trana, where a gauging station of the hydrometric network of the Environmental Protection Agency (ARPA) of the Piemonte Region monitors mean daily streamflow (Figure 1). Operating for over 20 years, this station provides valuable insights into local hydrology. From 1 January 2003 to 31 December 2023, the mean discharge was approximately 3.00 m^3/s, corresponding to the 28th percentile of the flow duration curve. The

10.1029/2025WR041133

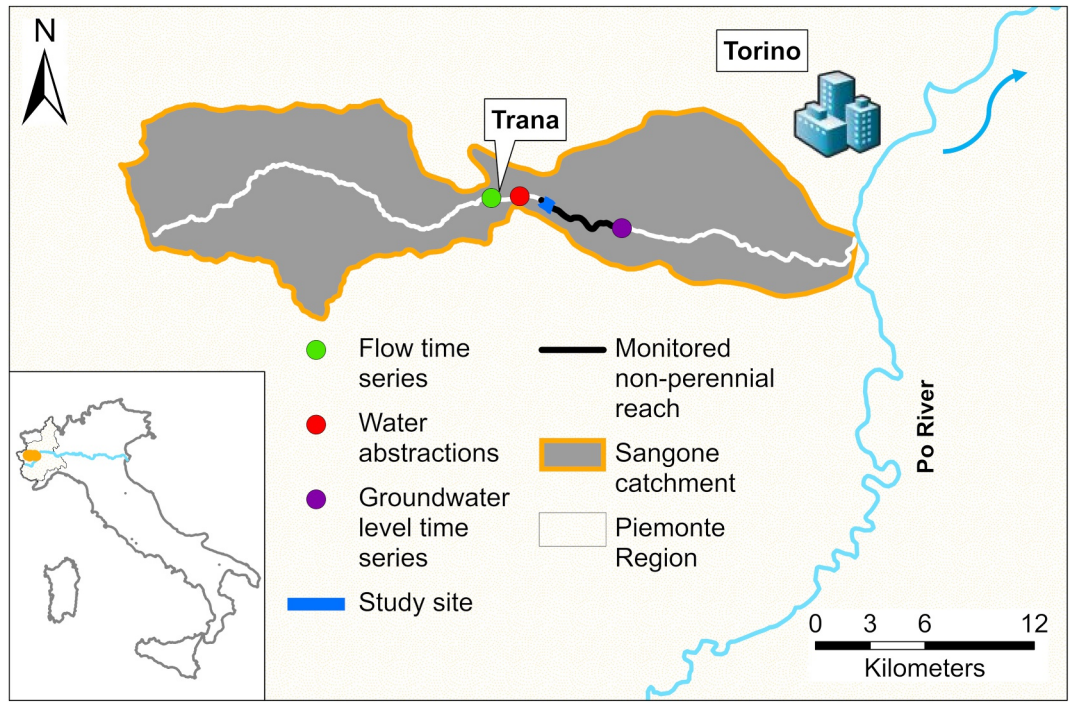

Figure 1. The study area (Northern Italy). The catchment (in gray) of the Sangone River (in white), which flows into the Po River (in azure), near the metropolitan city of Torino. The locations of the flow time series from the Trana gauging station (green dot), surface water and groundwater abstractions (red dot), and groundwater level time series from the observation well (purple dot) are reported. The study site is marked by a blue line, while the monitored non-perennial reach is shown in black. The main flow direction is indicated by the blue arrow.

bankfull discharge (sensu Leopold et al., 1964), approximated as the 2-year flood, is 34.50 m^3/s, while minimum flows rarely drop below 0.44 m^3/s (97th percentile). No zero-flow events have been recorded. Peak discharges typically occur in spring (April–June) and autumn (October–November), low-flow conditions dominate in winter (January–March) and summer (July–September) months. Since March 2014, an observation well of the environmental monitoring network of the Metropolitan City of Turin, located at the end of the selected reach (~8 km downstream of the Trana section), has been monitoring daily groundwater levels (Figure 1). Until 31 December 2023, the mean groundwater level was 8.11 m below ground level, with minimum and maximum values of −14.26 and −6.26 m, respectively.

In the upper part of the Sangone, characterized by a perennial hydrologic regime, primary pressure on the fluvial ecosystem arises from water abstraction for hydropower generation. However, these withdrawals originate from small diversion weirs with minimal storage capacity, and return the water to the river upstream of the Trana section, therefore their effect on the monitored reach can be considered negligible, and the gauging station measurements reflect the natural flow regime. In the downstream part, below the village of Trana, hydromorphological impacts escalate significantly due to the presence of agricultural water diversions and groundwater abstractions (Figure 1). In this lower segment, before joining the Po River, prolonged flow intermittency can occur, particularly in summer when water is highly withdrawn for crop irrigation. However, no reliable data exist on the actual volumes of water withdrawn by these diversions, making it difficult to accurately quantify their impact on the natural flow regime.

The study area is located in the middle part of the Sangone catchment, just below the water abstractions located in the vicinity of the village of Trana (Figure 1). In the monitored non-perennial reach, river banks are not confined and the river planform corresponds to a sinuous with alternate bars morphology characterized by some multithread sections (Gurnell et al., 2014). For the MesoHABSIM application, a 450-m-long sub-reach (the study site, Figure 2) was selected. It has a mean slope of 1% and spans a length between 10 and 20 times the average channel width, as recommended by Vezza et al. (2017).

19447973, 2026, 3, Downloaded from https://agupubs.onlinelibrary.wiley.com/doi/10.1029/2025WR041133 by Politecnico Di Torino Sist. Bibl Del Polit Di Torino, Wiley Online Library on [07/10/2026]. See the Terms and Conditions (https://onlinelibrary.wiley.com/terms-and-conditions) on Wiley Online Library for rules of use; OA articles are governed by the applicable Creative Commons License

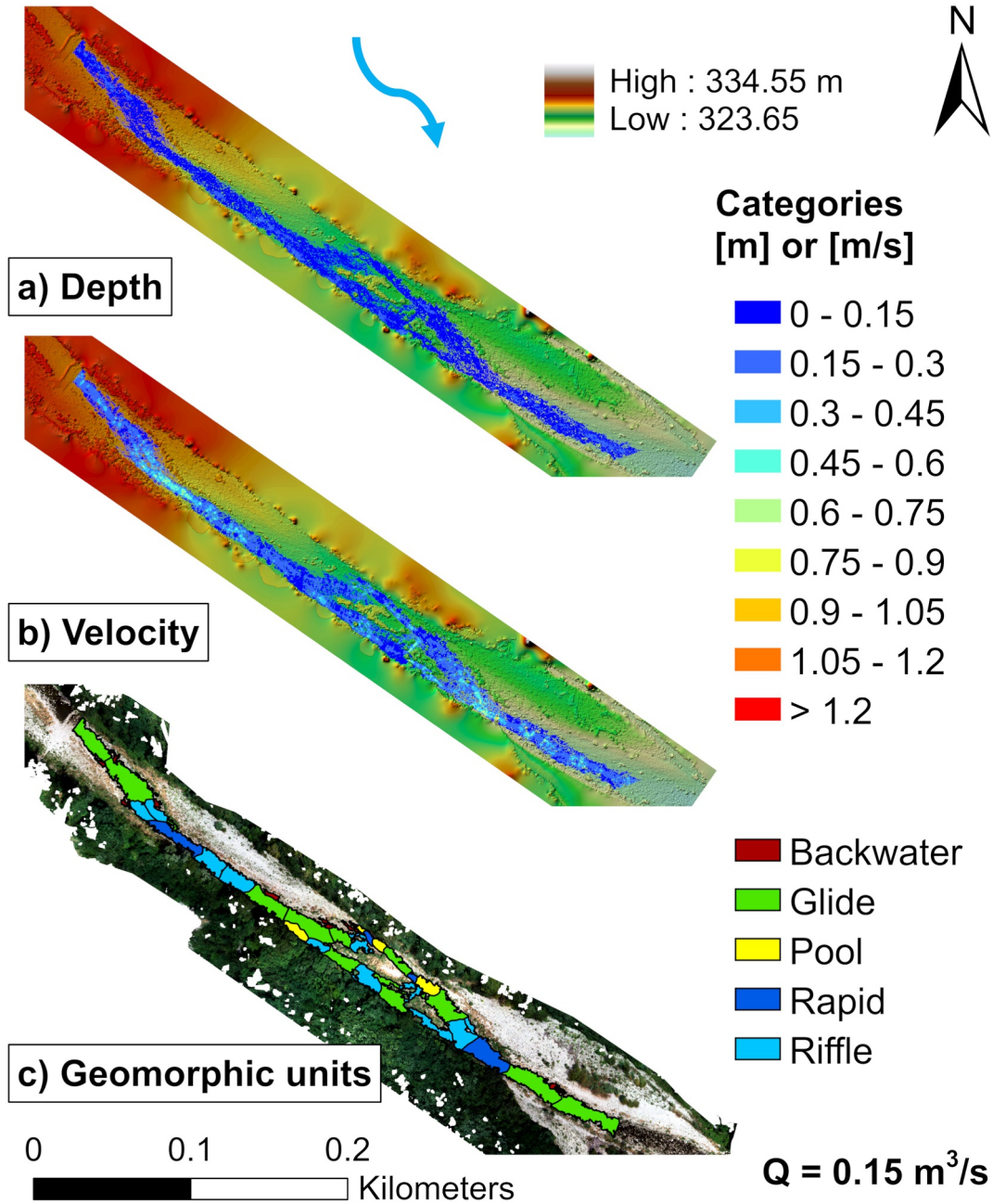

Figure 2. Simulation results for (a) water depth and (b) velocity under the flow condition observed during the UAS flight ($Q = 0.15$ m^3/s), utilizing the bathymetrically-corrected DEM as background. Depth and velocity are color-coded according to the corresponding categories of the MesoHABSIM approach (Table 1), ranging from the smallest (in blue) to the highest (in red). (c) Corresponding GUs mosaic overlaid on the RGB orthomosaic collected during the field survey of 12 July 2021. The GUs are color-coded following the standardized scheme adopted in the SimStream-Web service. The main flow direction is indicated by the blue arrow.

2.2. Habitat Description

The meso-scale habitat model, MesoHABSIM (Parasiewicz, 2007), is a methodological approach designed to model aquatic habitats using GUs (such as pools, glides and riffles, Belletti et al., 2017) as spatial unit of analysis. MesoHABSIM is characterized by a specific data collection strategy and analytical techniques that allow computing the habitat availability for target species under variable discharge conditions (Vezza, Parasiewicz,

19447973, 2026, 3, Downloaded from https://agupubs.onlinelibrary.wiley.com/doi/10.1029/2025WR041133 by Politecnico Di Torino Sist. Bibl Del Polit Di Torino, Wiley Online Library on [07/10/2026]. See the Terms and Conditions (https://onlinelibrary.wiley.com/terms-and-conditions) on Wiley Online Library for rules of use; OA articles are governed by the applicable Creative Commons License

19447973, 2026, 3, Downloaded from https://agupubs.onlinelibrary.wiley.com/doi/10.1029/2025WR041133 by Politecnico Di Torino Sist. Bibl Del Polit Di Torino, Wiley Online Library on [07/10/2026]. See the Terms and Conditions (https://onlinelibrary.wiley.com/terms-and-conditions) on Wiley Online Library for rules of use; OA articles are governed by the applicable Creative Commons License

Table 1
The Physical Habitat Attributes Considered by the MesoHABSIM Approach for the Geomorphic Units' Characterization

Habitat parameter	Units	Number of categories	Categories/Description
Geomorphic units (GUs) type	Yes/no	18	Pothole, Cascade, Rapid, Riffle, Step, Pool, Glide, Dune, Aquatic vegetation, Secondary channel, Flood lake, Wetland, Artificial element, Waterfall, Plunge pool, Backwater, Rock glide, Isolated pond
GU gradient	%	1	Water surface mean gradient of the GU
GU longitudinal connectivity	Yes/no	1	Habitat binary attribute describing mesohabitats longitudinal river connectivity
Depth	Percentage of samples	9	Categories in 0.15 m increments (range 0.0–1.20 m and above)
Velocity	Percentage of samples	9	Categories in 0.15 m/s increments (range 0.0–1.20 m/s and above)
Substrate	Percentage of random samples	12	gigalithal (rocks), megalithal (>40 cm), macrolithal (20–40 cm), mesolithal (6–20 cm), microlithal (2–6 cm), akal (gravel > 0.2 cm), psammal (sand), pelal (silt and clay), detritus (organic matter), xylal (woody debris, roots), sapropel (dark anoxic mud), phytal (submerged plants)
Cover	Yes/no	9	Boulders, canopy shading, overhanging vegetation, roots, submerged vegetation, emerging vegetation, undercut banks, woody debris, shallow margins
Froude number	(Flow velocity)/(9.81*depth)$^{0.5}$	1	Average over the GU area
Flow velocity standard deviation (SD)	m/s	1	SD over GU area

Note. For each habitat parameter, the corresponding categories are expressed as reported in Vezza et al. (2017).

Spairani, & Comoglio, 2014). It provides habitat time-series, employable to predict the magnitude and duration of stressful events for the aquatic fauna (Koutrakis et al., 2019; Parasiewicz, Rogers, et al., 2013).

The fluvial habitat description is achieved by analyzing specific physical attributes collected in the field (Vezza et al., 2017), which can be supplemented with remotely acquired data and outputs from 2D hydrodynamic models (e.g., Farò et al., 2022). These physical attributes include both abiotic (water depth, flow velocity, and sediment composition) and biotic (biotic substrate, cover, and shelter availability) factors (Table 1). To quantify available habitat for target species, habitat suitability criteria (HSC, e.g., Negro et al., 2023; Pinna et al., 2024) are applied to each GU under monitored flow conditions. The rank of suitability of each mesohabitat is determined based on the GU's physical attributes, which are evaluated against specified variable ranges considered in the HSC. For freshwater fish and macroinvertebrates, these criteria are typically defined by analyzing empirical data on species' presence and abundance at the mesohabitat scale using machine learning techniques (e.g., Costarrosa et al., 2022; Vezza, Parasiewicz, Calles, et al., 2014).

For fish species, the application of the HSC classifies the mesohabitats as unsuitable (if the fish species is predicted as absent), suitable (fish species predicted as present) or optimal (fish species predicted as abundant). The available habitat (H_A) is then computed for each surveyed flow condition (Q) using the following equation (Vezza et al., 2017):

$$H_{A,Q}(\%) = \sum_{i=1}^{N} \frac{\Omega_{i,Q}}{\Omega_{\max}} * k_{i,Q} \quad (1)$$

where, Ω_i is the area of the i-th mesohabitat (m^2) under flow condition Q, and Ω_{max} is the maximum wetted area of the selected river reach (m^2) at the highest monitored flow condition. The coefficient k reflects the level of suitability: it is set to 0 for GUs predicted as unsuitable, 0.25 for suitable GUs, and 0.75 for optimal GUs.

For macroinvertebrates, the habitat suitability is expressed through the Flow-T index (Laini et al., 2022), which ranges from 0 (completely lentic GU) to 1 (highly lotic GU), and can be predicted using the HSC developed by our research group (Pinna et al., 2024). The available habitat (H_A) is then quantified as the weighted mean value of the Flow-T index (FlowT) for each monitored flow condition (Q) using the following equation (Pinna et al., 2024):

$$H_{A,Q} = \sum_{i=1}^{N} \frac{\Omega_{i,Q}}{\Omega_{\max}} * \mathrm{Flow}T_{i,Q} \quad (2)$$

where, FlowT_i is the Flow-T index assigned to the i-th mesohabitat under flow condition Q, Ω_i is its area (in m^2), and Ω_{max} represents the maximum wetted area of the selected river reach (m^2) under the highest monitored flow condition.

To characterize the fluvial habitat, a systematic field data collection campaign was conducted to obtain high-resolution spatial information of the surveyed sub-reach. UAS data and the Structure from Motion technique were employed to reconstruct both the RGB orthomosaic (2 cm pixel size) and the corresponding Digital Elevation Model (DEM; 5.4 cm pixel size) of the study site (Figure 2). One hundred sixty-six off-nadir images (−10° tilt to avoid light reflectance from the water surface) were captured using a DJI Phantom 4 Pro RTK quadcopter equipped with an FC6310R camera. The UAS flight was conducted on 12 July 2021, at an average height of 60 m, during low water levels. Data processing was performed using Metashape software (Agisoft, St. Petersburg, Russia), following a standard workflow for river applications (e.g., Woodget et al., 2015). Four ground control points, distributed across the study area and measured using a dual-frequency Global Navigation Satellite System (GNSS) receiver in Real-Time Kinematic (RTK) mode, served as checkpoints for the 3D model validation. Errors on the checkpoints were 0.01, 0.03, and 0.03 m on the east, north and up components, respectively.

Given challenges in accurately capturing submerged riverbed elevations from photogrammetric data due to light refraction at the air-water interface (e.g., Dietrich, 2017; Murase et al., 2008; Tewinkel, 1963), a bathymetric correction was performed on the DEM using GIS tools (e.g., Lingua et al., 2023). The submerged surface was reprojected to correct for overestimations of elevation using a simple approach based on Snell's law (e.g., Yudha Partama et al., 2017). Given generally shallow water depths at the surveyed flow conditions (maximum measured depth = 0.38 m), a linear mono-parametric model with a slope of 1.33 was assumed for the bathymetric correction. This resulted in a bathymetrically-corrected DEM suitable for developing the 2D hydrodynamic model.

During the UAS flight, a river survey according to the MesoHABSIM protocols (e.g., Vezza et al., 2017) was further performed. In this way, the mosaic of GUs was outlined under the observed flow conditions ($Q = 0.15$ m^3/s) and supplemented with details on local cover presence and substrate composition. Specifically, GUs were delineated and stored in a GIS environment by walking downstream, and their local habitat attributes (GU type, GU longitudinal connectivity, and presence of fish cover, Table 1) were annotated. Coming back upstream, substrate composition was assessed by identifying the dominant granulometry at a minimum of 10 points per GU, following the categories adopted in the MesoHABSIM approach (Table 1; Vezza et al., 2017). Additionally, georeferenced information on water depth and current velocity was also collected above 60 points within the study site using an OTT MF Pro flow meter (Ott HydroMet, Kempten, Germany), and a dual band GNSS receiver.

Water depth and depth-averaged velocity distributions within GUs were simulated using a 2D fixed-bottom numerical model developed with HEC-RAS (Hydrologic Engineering Center of U.S.A, Davis, California, Version 5.0.7) software. The bathymetrically-corrected DEM served as input geometry for model construction. To determine the appropriate mesh resolution for the model, three grid configurations were explored (i.e., 0.0625, 0.25, and 1 m^2). Following Célik et al. (2008), a grid convergence (GC) analysis was performed to assess discretization uncertainty in water surface elevation (WSE), depth, and velocity. The results showed excellent convergence for WSE (median GC Index <0.1%), while depth and velocity were more sensitive to mesh refinement, particularly in shallow and near-bank areas. Nevertheless, habitat availability for all ecological targets varied by less than 0.7% among grid configurations, with no difference for fish species between the 0.25 and 0.0625 m^2 mesh sizes. Balancing numerical accuracy and computational efficiency, the 0.25 m^2 mesh was finally selected for the model's calibration and subsequent habitat analysis. Model's calibration involved adjusting the Manning's coefficient to achieve optimal agreement between simulated and observed WSE (Tonina & Jorde, 2013). The observed WSE was derived using Kriging interpolation by combining the RGB orthomosaic with the DEM generated with Metashape (Lingua et al., 2023). The discharge measured during the UAS survey ($Q = 0.15$ m^3/s) was used for model calibration (Figure 2). Eleven Manning's values (n) ranging from 0.040 to 0.050 were tested, with the best fit obtained for a value of 0.045, resulting in a root mean square error (RMSE) of

19447973, 2026, 3, Downloaded from https://agupubs.onlinelibrary.wiley.com/doi/10.1029/2025WR041133 by Politecnico Di Torino Sist. Bibl Del Polit Di Torino, Wiley Online Library on [07/10/2026]. See the Terms and Conditions (https://onlinelibrary.wiley.com/terms-and-conditions) on Wiley Online Library for rules of use; OA articles are governed by the applicable Creative Commons License

19447973, 2026, 3, Downloaded from https://agupubs.onlinelibrary.wiley.com/doi/10.1029/2025WR041133 by Politecnico Di Torino Sist. Bibl Del Polit Di Torino, Wiley Online Library on [07/10/2026]. See the Terms and Conditions (https://onlinelibrary.wiley.com/terms-and-conditions) on Wiley Online Library for rules of use; OA articles are governed by the applicable Creative Commons License

0.035 m and an R^2 exceeding 0.99. The selected Manning's coefficient was kept constant above the entire domain, as under the investigated discharge conditions, submerged areas were entirely confined within the active channel. Furthermore, sensitivity tests using spatially variable roughness across different substrate patches showed no significant effect on habitat availability (e.g., Pasternack et al., 2004). Once calibrated, the model was applied to simulate four discharges (i.e., 0.15, 1.00, 2.00, 3.00 m^3/s) under steady-state conditions, representing flow percentiles from the 99th to the 28th of the time series recorded in Trana, to describe the aquatic habitat in the surveyed sub-reach.

In addition to the four F conditions simulated with the hydrodynamic model, habitat characteristics were also derived for the first day after flow cessation (P condition), by assuming a linear recession of the wetted area over time between flow interruption and complete drying. To estimate the extent of wetted areas under this condition, the corrected DEM was artificially filled to simulate water accumulation in the lowest topographic depressions using GIS tools. The subsequent satellite-based analysis was then leveraged to (a) validate the assumption of a linear decline in wetted area after flow cessation, and (b) qualitatively verify the extent of the modeled wetted areas on the first day of the P condition, represented by a framing of isolated ponds.

As required by the MesoHABSIM approach, GU mosaics for the five simulated conditions (4 F and 1 P) were outlined and characterized with all their local habitat attributes (Table 1). Specifically, the field-collected information (e.g., GUs distribution, substrates and covers distribution) was synergistically integrated in a GIS environment with high-resolution data represented by the RGB orthomosaic, the bathymetrically-corrected DEM, and the simulated water depths and velocities. Such information was finally formatted according to the input requirements of the SimStream-Web service.

Concurrently with the UAS survey, an electrofishing campaign was further conducted at the study site following the Italian protocols for wadable rivers (i.e., Balzamo & Martone, 2014). This survey provided updated information on the local fish community composition, as available data were mostly limited to outdated studies (e.g., Badino et al., 2002), and supported the selection of appropriate ecological targets for habitat assessment. A total length of 150 m was analyzed using backpack electrofishing (model ELT60 IIGI 1.3 kW; DC voltage 300–500 V; frequency ≤30 Hz) by sampling different GUs identified and described at the current flow condition. To minimize handling stress, fish captured in each GU were immediately identified, classified into adult and juvenile life stages, and released back into the same mesohabitat. During temporary holding, water was partially replaced and aerated by an operator to ensure fish welfare. The observed fish species were Italian vairone (*Telestes muticellus*), Padanian goby (*Padogobius bonelli*), Italian chub (*Squalius squalus*), Italian barbel (*Barbus plebejus*), Italian minnow (*Phoxinus lumaireul*), and Italian brook barbel (*Barbus caninus*).

As ecological targets for applying the MesoHABSIM approach to monitored NPRs reach, two native fish species, adult and juvenile *T. muticellus* and adult *P. bonelli*, and the macroinvertebrate community (i.e., Flow-T index) were selected to account for both rheophilic and benthic organisms. The choice of these target fish was informed by the electrofishing survey and by the availability of HSC for Italian freshwater fauna. The HSC for these targets are included in the national library supported by the Italian National Institute for Environmental Protection and Research (ISPRA) and are accessible through the SimStream-Web service, which provides a comprehensive collection of HSC sets for native Italian freshwater species. Specifically, the HSC used in this study were developed by our research group using machine learning techniques applied to empirical species data collected at multiple sites across the Alpine and Apennine regions of Italy over several years (e.g., Pinna et al., 2024; Vezza, Parasiewicz, Calles, et al., 2014). The selected HSC, presented in Figures S1–S4 in Supporting Information S1, were then applied via SimStream-Web to quantify aquatic habitat availability in the study site under five simulated conditions, using Equations 1 and 2. An overview of the data acquisition and analysis workflow implemented in this study is illustrated in Figure 3.

2.3. Hydrological Characterization

To accurately describe aquatic habitat variation in the monitored NPRs reach, a satellite-based analysis was conducted to investigate the local hydrological regime, with a specific focus on the frequency and duration of flow intermittency. For this purpose, S2 and PS multispectral images and high-resolution images (HRIs), including the RGB orthomosaic and available Google Earth imagery, were integrated with locally recorded streamflow and groundwater level data to estimate the occurrences and durations of the P and D conditions over 7 years (2017–2023). The derived information was used to (a) define the amount of time over which wetted areas progressively

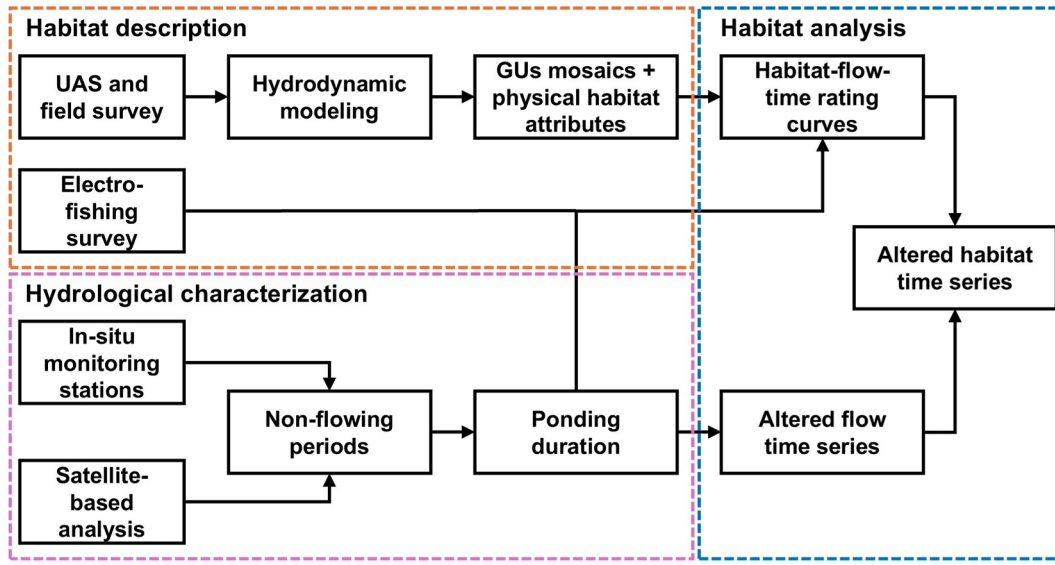

Figure 3. Workflow summarizing the data acquisition and analysis performed in this study. The process is structured into three interconnected components: habitat description (orange), hydrological characterization (magenta), and habitat analysis (blue).

contract to zero (i.e., P durations), necessary for assessing habitat dynamics during NF phases, and (b) identify the most severe drought periods within the monitored timeframe, representing critical windows for focusing habitat assessment efforts.

For satellite-based analysis, the methodology proposed by Cavallo et al. (2022) was employed. This approach allows the detection of surface water presence in NPRs through supervised analysis of False Color Images (FCIs) created using specific S2 band combinations. In this way, hydrological conditions (F, P, or D), in sufficiently wide NPR reaches (~30 m) that are not covered by a vegetation dome, can be identified and associated with satellite image acquisition dates. In this study, to increase observation frequency, the same methodology was adapted and employed for PS imagery.

S2, a mission of the European Space Agency, comprises three twin sun-synchronous satellites: Sentinel-2A (operational since 2015), Sentinel-2B (operational since 2017), and Sentinel-2C (operational since 2024). Together, they provide a revisit time of up to 2–3 days, acquiring images in 13 spectral bands in the visible (Red-Green-Blue), near-infrared (NIR), and shortwave infrared (SWIR) ranges, with a GSD of 10–60 m. The FCIs proposed by Cavallo et al. (2022) for S2 images are based on SWIR-NIR-Red bands (B11-B8-B4, Table 2).

The PS constellation, operated by Planet Labs (San Francisco, CA, USA), consists of over 150 sun-synchronous CubeSats launched since 2013. These satellites, equipped with three different sensor generations, acquire imagery in visible and NIR wavelengths (4–8 spectral bands), with almost a daily revisit time and a resampled GSD of 3 m (Frazier & Hemingway, 2021; Roy et al., 2021). Due to the absence of SWIR bands, a modified false-color

Table 2
Sentinel-2 and PlanetScope Spectral Band Characteristics, and Corresponding Ground Sample Distance (GSD), Used for Composing False-Color Images

Sentinel-2		PlanetScope	
Band number	Wavelength range [nm]; GSD [m]	Band number	Wavelength range [nm]; GSD [m]
B11 (SWIR)	1565–1655; 20	B3 (Red)	590–670; 650–682; 650–680; ~3
B8 (NIR)	785–899; 10	B4 (NIR)	780–860; 846–888; 845–885; ~3
B4 (Red)	650–680; 10	B1 (Blue)	455–515; 464–517; 465–515; ~3

Note. For PlanetScope, wavelength ranges correspond to three sensors generations, each with slight variations (Frazier & Hemingway, 2021).

19447973, 2026, 3, Downloaded from https://agupubs.onlinelibrary.wiley.com/doi/10.1029/2025WR041133 by Politecnico Di Torino Sist. Bibl Del Polit Di Torino, Wiley Online Library on [07/10/2026]. See the Terms and Conditions (https://onlinelibrary.wiley.com/terms-and-conditions) on Wiley Online Library for rules of use; OA articles are governed by the applicable Creative Commons License

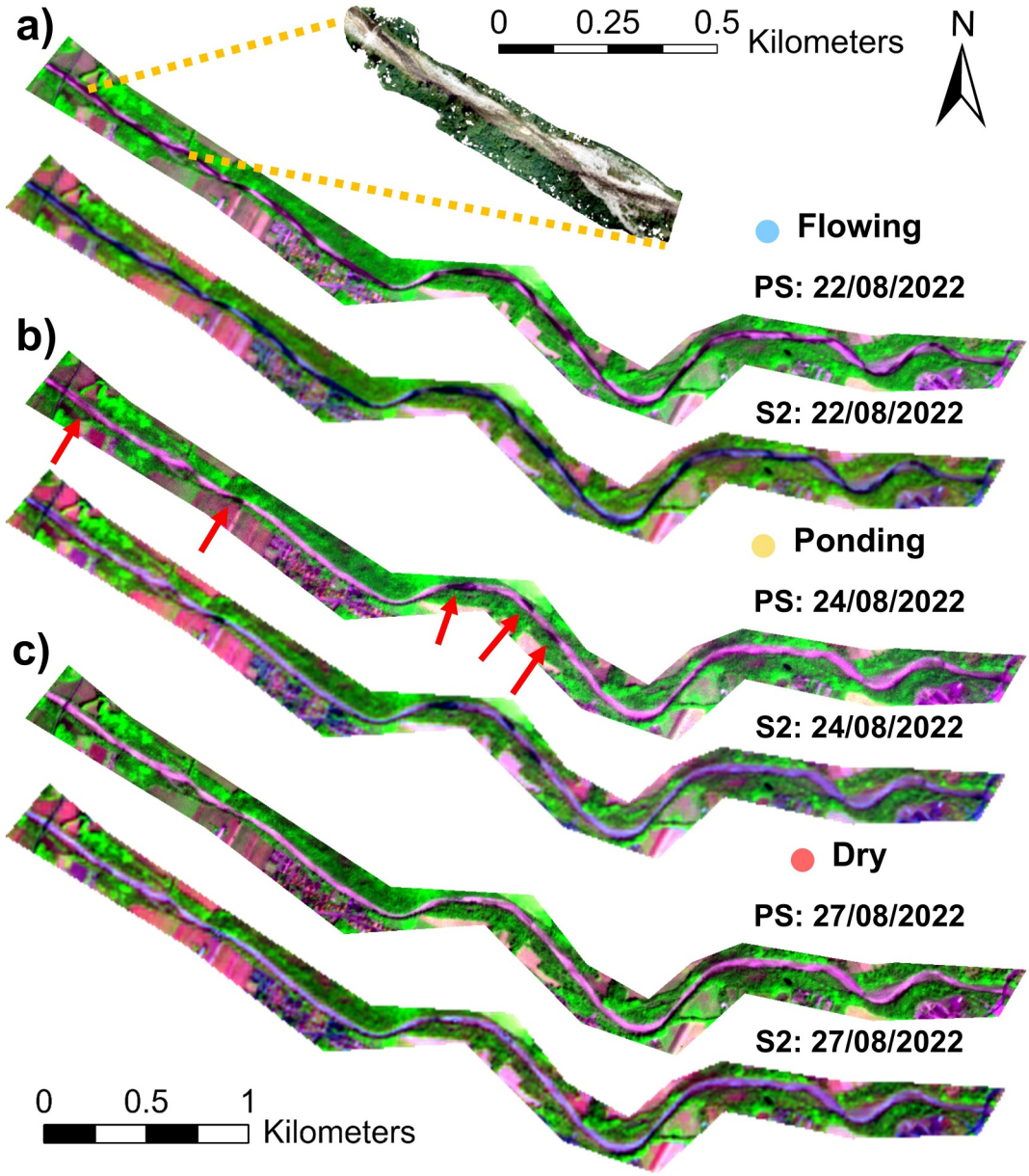

Figure 4. Sentinel-2 (S2, B11-B8-B4, below) and PlanetScope (PS, B3-B4-B1, above) false-color images corresponding to (a) flowing (22 August 2022), (b) ponding (24 August 2022), and (c) dry (27 August 2022) conditions during the most severe drought event of summer 2022. The RGB orthomosaic representing the surveyed sub-reach is depicted on the top of the image. The red arrow highlighted the residual wetted areas during the ponding condition on 24 August 2022.

combination using Red-NIR-Blue bands (B3-B4-B1, Table 2) was identified to maximize the possibility of distinguishing water from other features in the river corridor. This combination was selected as (a) two bands (namely B3 and B4) are in the same wavelength range of the ones used for S2 (respectively B4 and B8, Table 2), and (b) it provided an equivalent shade of colors (Figure 4). Validation of this approach was carried out through comparisons of PS FCIs with S2 and HRIs imagery with identical or closely matching acquisition dates. Specifically, consistency in hydrological condition assessments was checked. Moreover, four field surveys performed during the summers of 2021 and 2022 served as reference observations to further evaluate the reliability of the proposed approach.

All available satellite images of the study area with low or no visibility obstructions (e.g., cloud cover or fog) were retrieved: S2 (Level 2A data set) via the geemap Python package (Wu, 2020), and PS via the Planet Explorer

19447973, 2026, 3, Downloaded from https://agupubs.onlinelibrary.wiley.com/doi/10.1029/2025WR041133 by Politecnico Di Torino Sist. Bibl Del Polit Di Torino, Wiley Online Library on [07/10/2026]. See the Terms and Conditions (https://onlinelibrary.wiley.com/terms-and-conditions) on Wiley Online Library for rules of use; OA articles are governed by the applicable Creative Commons License

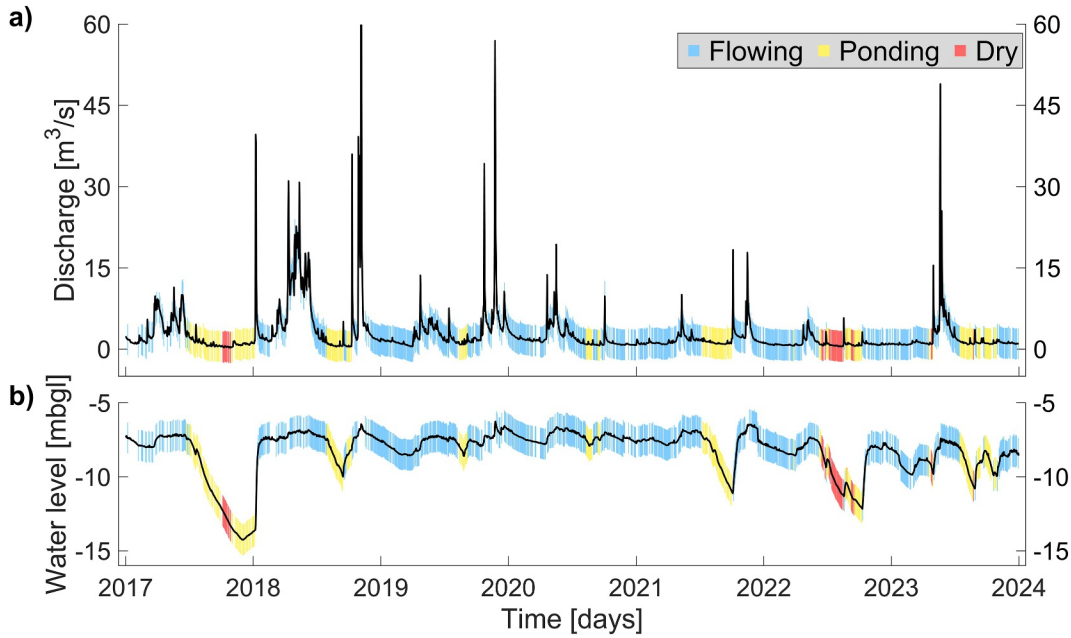

Figure 5. Time series of (a) flow (recorded at Trana) and (b) groundwater level (registered by the observation well) during the monitored period (1 January 2017–31 December 2023). The satellite-derived hydrological conditions are presented by vertical lines in blue (flowing condition), yellow (ponding condition), and red (dry condition). The most severe drought period corresponding to summer 2022 can be clearly identified. All related data are provided in Table S1.

platform (https://www.planet.com/explorer/). For each image, FCIs were generated in a GIS environment by combining the identified bands from each sensor (Table 2). These FCIs were then processed through a supervised classification procedure to assign the hydrological conditions (F, P, or D).

Due to surface water and groundwater abstractions occurring between the gauging station and the monitored reach (Figure 1), the flow time series recorded in Trana (i.e., the natural streamflow) does not represent the flow rate in the study site (i.e., the altered streamflow). However, the absence of reliable data on water volumes withdrawn (or released) at the agricultural weirs, and on the timing of diversions operations, precluded reconstructing the altered flow regime over the entire monitored period (2017–2023). Additionally, considerable interannual variability between discharge (or groundwater levels) and the occurrence of different hydrological conditions further limits long-term reconstructions (e.g., multiyear; see Figures S5 and S6 in Supporting Information S1). To address this, we adopted a conservative approach, restricting the analysis to the most critical period (t_C) for aquatic habitat availability. Specifically, we considered the 1 June–30 October interval of each year, when withdrawals for irrigation intensify during the main summer crop season in Northern Italy (Azar et al., 2016), and when the satellite-based analysis indicated the highest occurrence of NF conditions. Within these windows, we then identified the most severe drought period, characterized by the greatest extent of the totally D condition. The altered streamflow during this period was then approximated (Figure 6b) and used as an example to perform a focused habitat analysis, representing the worst-case scenario for aquatic habitat availability.

To approximate the altered flow time series during this critical period, we analyzed the relationship between discharges at Trana, groundwater levels in the observation well, and the hydrological conditions derived from supervised classification (Figure S6 in Supporting Information S1). First, we assessed the predictive ability of discharges at Trana to distinguish between F and NF phases (binary classification) during summer periods using a Receiver Operating Characteristic (ROC) curve and associated Area Under the Curve (AUC). Next, we applied the Youden Index (e.g., Fluss et al., 2005) to the ROC curve of the most severe drought period, obtaining a threshold discharge value (Q^*) that optimally separated F and NF conditions in the monitored reach. This threshold represents the maximum discharge recorded at Trana below which NF conditions (P or D) were consistently observed in the monitored reach during the most severe drought period. As natural flow remained relatively stable during this critical period (Figure 6b), based on the supervised classification of satellite images we assumed that abstraction and release patterns were likewise stable, and therefore treated Q^* as a constant

19447973, 2026, 3, Downloaded from https://agupubs.onlinelibrary.wiley.com/doi/10.1029/2025WR041133 by Politecnico Di Torino Sist. Bibl Del Polit Di Torino, Wiley Online Library on [07/10/2026]. See the Terms and Conditions (https://onlinelibrary.wiley.com/terms-and-conditions) on Wiley Online Library for rules of use; OA articles are governed by the applicable Creative Commons License

19447973, 2026, 3, Downloaded from https://agupubs.onlinelibrary.wiley.com/doi/10.1029/2025WR041133 by Politecnico Di Torino Sist. Bibl Del Polit Di Torino, Wiley Online Library on [07/10/2026]. See the Terms and Conditions (https://onlinelibrary.wiley.com/terms-and-conditions) on Wiley Online Library for rules of use; OA articles are governed by the applicable Creative Commons License

threshold. Indeed, during drought periods with minimal precipitations, agricultural water diversions in Northern Italy usually operate at their maximum capacity, withdrawing all available water up to the licensed volume while releasing a minimum flow (Santato et al., 2016). Based on this, Q^* was used to define the altered flow time series (Q_{Altered}) through the following system of equations:

$$\begin{cases} Q_{\text{Altered}}(t_C) = Q_{\text{Natural}}(t_C) - Q^*, & Q_{\text{Natural}}(t_C) > Q^* \\ Q_{\text{Altered}}(t_C) = 0, & Q_{\text{Natural}}(t_C) \le Q^* \end{cases} \tag{3}$$

where, Q_{Natural} is the mean daily discharge recorded at the Trana gauging station during the identified critical period (t_C). In this framework, all diversions and abstractions downstream of the Trana section (Figure 1) can be idealized as a single main water diversion with a minimum release that produces zero-flow at the study site, and a maximum withdrawal capacity equal to Q^*. To further test the reliability of this analysis, the resulting altered flow time series in terms of hydrological conditions was validated against the satellite-derived hydrological classification.

2.4. The New SimStream-Web Module for NPRs (NPRs-Module)

In NPRs, aquatic habitat varies with flow rate during F phase and with time during the NF periods (Acuña et al., 2020). To account for the interplay between flow, time and habitat availability, the innovative NPRs-module of the MesoHABSIM approach introduces a specific rating curve able to simultaneously consider the intermittent behavior of aquatic habitat availability. This curve directly derives from the traditional habitat-flow rating curve of common habitat models, by adding a second quadrant to the graph. This second quadrant accounts for the recession of wetted area and habitat availability with respect to the amount of time elapsed after flow cessation (Negro et al., 2019). The resulting curve is then called habitat-flow-time rating curve (Figure 6a). Specifically, the habitat values computed using Equations 1 and 2 for each considered flow condition are interpolated using a mathematical spline function to generate the habitat-flow-time rating curves for the selected ecological targets.

The definition of this curve allows the generation of the habitat time-series for NPRs, enabling the analysis of the spatio-temporal variation of aquatic habitat availability during both F and NF phases. Specifically, a daily flow time series can be converted into habitat time series by means of the following system of equations:

$$\begin{cases} H_A(t) = H(Q(t)), & Q > 0 \\ H_A(t) = H(T), & Q = 0 \end{cases} \tag{4}$$

where, $H(Q(t))$ represents the habitat availability, for a given ecological target, corresponding to the streamflow $Q(t)$ at time t, while $H(T)$ defines the habitat availability as a function of T, the time elapsed since flow ceased.

According to Equation 4, the altered flow time series (Figure 6b), derived from the hydrological characterization, was converted into habitat terms using the habitat-flow-time rating curves (Figure 6a), to evaluate the spatio-temporal evolution of aquatic habitat in the monitored reach for the considered ecological targets during the most severe drought period (Figures 6c–6e).

To facilitate habitat modeling in NPRs and support the definition of e-flows in regulated non-perennial reaches, the new NPRs-module has been developed and it is freely available to users through the SimStream-Web service (Version 1.1.0; Politecnico di Torino (DIATI), 2024) on the web page of the Italian National Institute for Environmental Protection and Research (ISPRA).

3. Results

3.1. Habitat Description

A total of 172 GUs were delineated and described across the five simulated conditions. Among these, 14 mesohabitats (8.1% of the total) were identified as isolated ponds, representing the remaining wetted areas during the P condition on the first day after flow cessation. Overall, glides comprised the majority of GUs (35.5%), followed by riffles (32.6%). Backwaters, rapids, and pools accounted for 10.5%, 9.3%, and 4.1%, respectively. The water

19447973, 2026, 3, Downloaded from https://agupubs.onlinelibrary.wiley.com/doi/10.1029/2025WR041133 by Politecnico Di Torino Sist. Bibl Del Polit Di Torino, Wiley Online Library on [07/10/2026]. See the Terms and Conditions (https://onlinelibrary.wiley.com/terms-and-conditions) on Wiley Online Library for rules of use; OA articles are governed by the applicable Creative Commons License

surface area of identified GUs varied significantly, ranging from a minimum of 1.8 m^2 (attributed to a backwater) to a maximum of 675.0 m^2 (attributed to a glide). Considering habitat attributes, water depths were generally shallow across all flow conditions. At the lowest flow condition ($Q = 0.15$ m^3/s), most depths were below 0.30 m (mean = 0.07 m, Figure 2). At the highest flow ($Q = 3.00$ m^3/s), depth values remained below 0.70 m (mean = 0.23 m). Conversely, flow velocities increased significantly with discharge, ranging from a mean of 0.20 m/s at 0.15 m^3/s to 0.68 m/s at 3.00 m^3/s. The riverbed substrate was dominated by mesolithal (49.6%), macrolithal (33.8%), and microlithal (14.9%), with psammal and pelal substrates contributing less than 1% each. Regarding fish cover and shelters, boulders were the most common feature, observed in 99.0% of GUs, followed by emerging vegetation (50.0% of GUs), shallow margins (41.3% of GUs), and canopy shading (37.2% of GUs). Water surface gradients across the mesohabitats ranged from 0.0 to 0.068.

3.2. Hydrological Characterization

The comparison of PS FCIs and HRIs, assumed as ground truth, demonstrated excellent agreement in distinguishing submerged and emerged areas, revealing a satisfactory level of correspondence (Figure 4). Specifically, in all cases (100%), the hydrological conditions identified in PS imagery matched those observed in the corresponding 12 available HRIs. Similarly, a perfect correspondence (100%) was also assessed when comparing 403 PS and S2 FCIs acquired in the same dates, as well as with the hydrological conditions observed during the four independent field surveys. Thus, the methodology for the supervised classification of hydrological condition proposed by Cavallo et al. (2022), and adapted for PS imagery, was considered suitable for the purposes of the study.

A total of 1,736 cloud-free satellite images from S2, PS, and HRI sources were classified as F, P, or D over the monitored period (1 January 2017–31 December 2023). The majority were PS images (1,057; 60.9% of total images), followed by S2 (667; 38.4%) and HRIs (12; 0.7%). This extensive data set allowed for an average of 189 hydrological condition observations per year, ranging from 122 in 2017 to 210 in 2019, which correspond to a very high effective revisit time of 1.93 days. Overall, F conditions predominated (73.8% of total images), followed by P (21.4%) and D conditions (4.8%). In the monitored reach, NF periods occurred annually but varied significantly in terms of duration and severity. For example, in 2019, the reach never dried out, with P lasting only 22 days. In contrast, complete drying occurred in 2017, 2022, and briefly (i.e., 5 days) in 2023 (Figure 5). Seasonal patterns indicated that NF conditions were most frequent during August and September (100% of monitored years). Additional occurrences were observed in July (71.4% of monitored years), October (57.1%), and June (28.6%). Rare NF events were detected in March and April (14.3%) at the end of the annual winter low flow period.

The relationship between the discharges at Trana or groundwater levels in the observation well and the occurrence of NF conditions detected via supervised classification did not exhibit a consistent pattern with P and D conditions that originated at different values depending on the year (Figure 5). Overall, as represented in Figure S5 in Supporting Information S1, P condition occurred at discharges ranging from 0.36 to 2.45 m^3/s (mean = 0.99 m^3/s) and groundwater levels ranging from −14.26 to −7.29 m (mean = −9.50 m). D conditions were associated with discharge values between 0.27 and 0.96 m^3/s (mean = 0.63 m^3/s) and groundwater levels ranging from −13.31 to −8.24 m (mean = −10.79 m). Analysis of P durations before transitioning to completely D conditions revealed six distinct events, lasting from 4 to 96 days. The median P duration was 8 days, which was assumed as representative of the time required for the monitored reach to dry out after flow ceased and incorporated into the second quadrant of the habitat-flow-time rating curves (Figure 6a).

By focusing on the summer periods from 2017 to 2023 (1 June–30 October) and reducing the analysis to a binary classification problem (F and NF), we found that discharges at Trana were generally a stronger predictor than groundwater levels, yielding an AUC of 0.91. Examining each individual summer period, the Youden Index was generally higher and more consistent when based on discharges at Trana, ranging from 0.73 in 2019 to 1.00 in 2017. In contrast, while groundwater levels produced the highest Youden Index values in 2019 (1.00) and 2020 (0.87), they also exhibited greater variability, dropping as low as 0.42 in summer 2022. Nevertheless, we observed significant interannual variability in the thresholds which distinguish the zero-flow periods (Figure S6 in Supporting Information S1). Specifically, for the F condition, the lower quartile (3rd quartile 75%) values for each year ranged from 1.01 to 3.04 m^3/s for discharge (mean = 1.65 m^3/s) and from −10.27 to −7.26 m for groundwater levels (mean = −7.72 m). While, for the NF phase, the upper quartiles (1st quartile 25%) exhibited

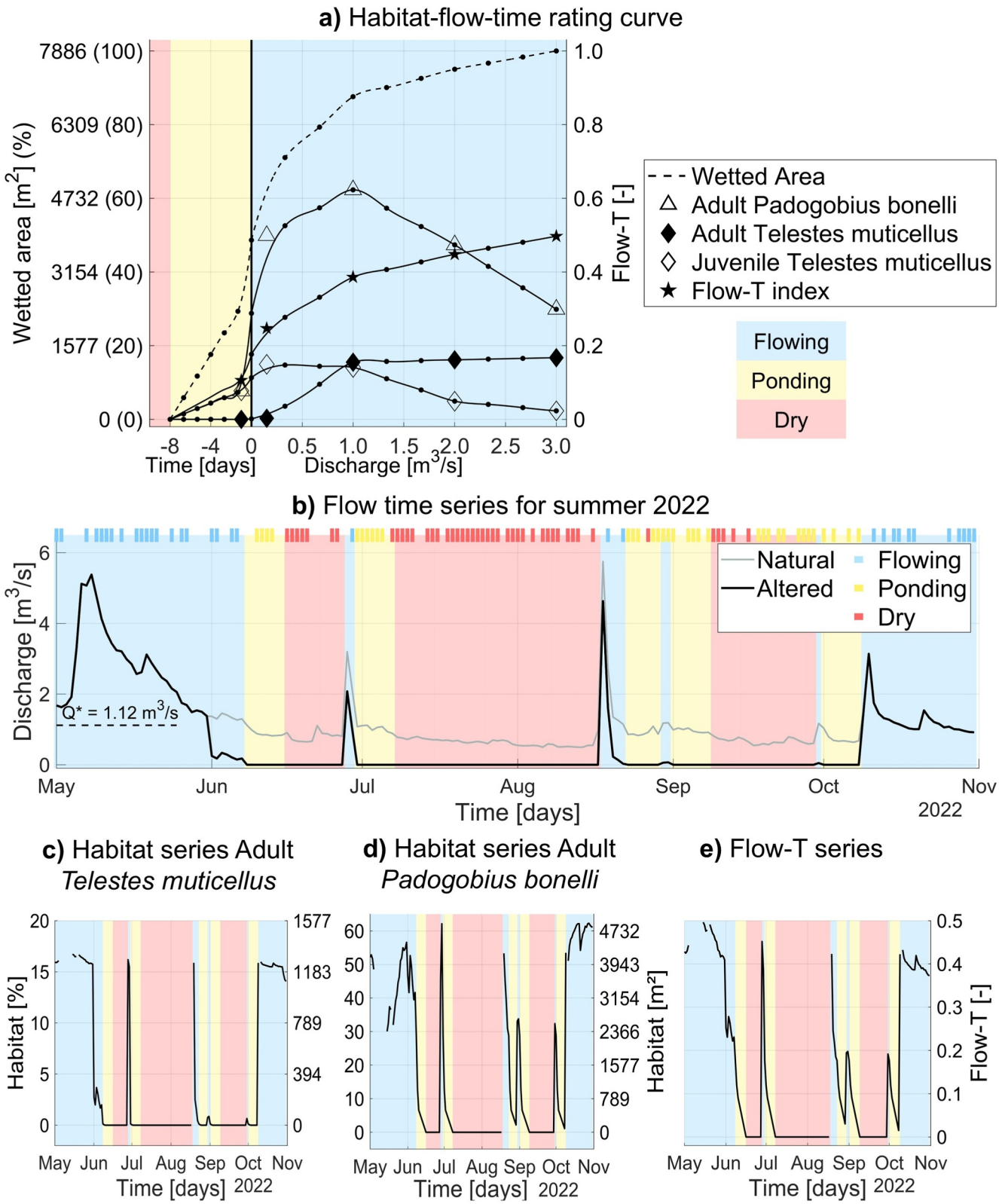

Figure 6.

19447973, 2026, 3, Downloaded from https://agupubs.onlinelibrary.wiley.com/doi/10.1029/2025WR041133 by Politecnico Di Torino Sist. Bibl Del Polit Di Torino, Wiley Online Library on [07/10/2026]. See the Terms and Conditions (https://onlinelibrary.wiley.com/terms-and-conditions) on Wiley Online Library for rules of use; OA articles are governed by the applicable Creative Commons License

19447973, 2026, 3, Downloaded from https://agupubs.onlinelibrary.wiley.com/doi/10.1029/2025WR041133 by Politecnico Di Torino Sist. Bibl Del Polit Di Torino, Wiley Online Library on [07/10/2026]. See the Terms and Conditions (https://onlinelibrary.wiley.com/terms-and-conditions) on Wiley Online Library for rules of use; OA articles are governed by the applicable Creative Commons License

slightly lower variability, ranging from 0.80 to 1.65 m^3/s for discharge (mean = 1.08 m^3/s) and from −9.28 to −7.51 m for groundwater levels (mean = −8.22 m). Overall, discharge showed higher variability during the F condition, particularly in 2018, when whiskers ranged from 0.58 to 10.62 m^3/s (median = 2.70 m^3/s), compared to the NF phase (maximum variability: 0.27–2.45 m^3/s in 2017). In contrast, groundwater levels exhibited the opposite pattern, with the greatest variability occurring during the NF phase compared to the F condition (maximum variability from −13.31 to −7.32 m in 2017).

Among the summer periods from 2017 to 2023, the drought of 2022 emerged as the most severe period for the monitored reach, with over 40 consecutive days of total D condition between July and August (Figure 5). This window was therefore selected as the critical period (t_C) for the habitat analysis. Specifically, the altered streamflow was defined from 1 June to 8 October, corresponding to the assumed duration of the crop irrigation season of 2022, as all satellite observations before and after this period indicated a F condition. During this period, by computing the Youden Index (i.e., 0.98) of the corresponding ROC curve, the optimal threshold discharge value (Q^*) which separated F and NF phases was estimated at 1.12 m^3/s (Figure 6b). Below Q^*, from 1 June to 8 October, all satellite images (100.0%) were consistently classified as P or D conditions. Moreover, a strong agreement was observed between the hydrological conditions derived from the satellite-based analysis and the resulting altered streamflow, with a classification accuracy of 85.1% across the three conditions (i.e., F, P, and D, Figure 6b).

3.3. Habitat Assessment in NPRs

The resulting habitat-flow-time rating curves revealed distinct trends for each ecological target (Figure 6a). For adult *T. muticellus*, habitat availability increased sharply from 0.15 to 1.00 m^3/s, reaching 15.5% of the maximum wetted area. Beyond this discharge, the curve plateaued, with habitat extent showing only a slight increase up to 3.00 m^3/s (16.7%). At low flows (e.g., 0.15 m^3/s) and during P conditions, habitat availability was minimal, approaching 0.0 m^2 (<1% of the wetted area). Conversely, juvenile *T. muticellus* exhibited peak habitat availability at 0.15 m^3/s (14.9% of the wetted area), with a progressive decline as flow increased, reaching 2.3% at 3.00 m^3/s. Residual habitat during the P condition covered 7.7% of the wetted area on the first day after flow cessation and persisted for up to 8 days before the sub-reach dried out. Adult *P. bonelli* displayed a similar trend to juvenile *T. muticellus*, although it showed the highest overall habitat availability among all targets. Habitat availability peaked at 1.00 m^3/s, covering 62.3% of the wetted area, with over 90% of GUs at this flow condition classified as optimal. However, habitat availability declined at higher discharges, dropping to 29.9% at 3.00 m^3/s. During the P condition, *P. bonelli* habitat contracted more gradually compared to juvenile *T. muticellus*. For macroinvertebrates, the Flow-T index showed a monotonic increase with discharge, ranging from 0.24 at 0.15 m^3/s to nearly 0.5 at 3.00 m^3/s. During the NF phase, the index maintained a relatively high value (>0.1) on the first day after flow cessation, exceeding values observed for any fish target, before steadily declining to zero as drying progressed.

The estimated altered flow time series for the monitored reach downstream of the water abstractions during summer 2022 is presented in Figure 6b. In Figures 6c–6e, the corresponding habitat time series for the adult stage of *T. muticellus* and *P. Bonelli*, and the Flow-T series are depicted, respectively. Over the considered period, four discharge events above Q^* (in late June, mid and late August, and late September, Figure 6b) temporarily restored the F condition in the monitored reach, before transitioning again to P and subsequently to D conditions. The shortest P condition duration, corresponding to 4 days, was observed in late August. Each discharge event produced a corresponding peak in the habitat series. According to the habitat-flow-time rating curves, habitat availability for adult *T. muticellus* dropped rapidly to zero immediately after flow cessation (Figure 6c), making it highly vulnerable to flow intermittency. In contrast, adult *P. bonelli* and the macroinvertebrate community

Figure 6. (a) Habitat-flow-time rating curves for the surveyed sub-reach, computed using SimStream-Web. The curves show the evolution of total wetted area (%) and available habitat for adult *Telestes muticellus* (filled diamonds), juvenile *T. muticellus* (open diamonds), adult *Padogobius bonelli* (triangles), and the Flow-T index (filled stars), as functions of discharge and time. The flowing condition is highlighted in blue, the ponding condition, estimated to stand for 8 days, in yellow, and the dry condition in red. (b) The natural (in gray) and the altered (in black) flow time series estimated from 1 June to 8 October 2022. Hydrological conditions derived from the satellite-based analysis are reported on the top of the graph using vertical lines. The altered habitat time series for (c) adult *T. muticellus* and (d) adult *P. Bonelli*, and (e) Flow-T series obtained via SimStream-Web. For discharges exceeding 3 m^3/s, habitat values could not be estimated and are represented as NaN (not-a-number) values.

exhibited a more gradual decline, reflecting their greater capacity to exploit residual aquatic habitats during NF periods (Figures 6d and 6e).

4. Discussion

4.1. Satellite Images Analysis

In an attempt to improve the temporal resolution in monitoring NPRs habitat dynamics, we adapted the S2 image-based approach proposed by Cavallo et al. (2022) to include PS imagery. Specifically, we replicated similar color schemes by combining specific bands (B11-B8-B4 for S2 and B3-B4-B1 for PS) to highlight water presence in river corridors. The primary difference in band selection for FCIs between S2 and PS lies in the replacement of the SWIR band with the Blue band in PS composites. While the SWIR band is particularly effective in differentiating water bodies from other land covers, it is not available in PS sensors, requiring alternative spectral configurations. Nevertheless, the introduction of a new generation of PS sensors since 2018 has improved spectral clarity (Frazier & Hemingway, 2021), aligning their acquisition bands more closely with S2 and allowing better integration of information collected with these systems (Table 2, Roy et al., 2021).

The integration of S2 and PS data sets effectively overcomes common limitations encountered in hydrological assessments for NPRs, offering high temporal and spatial resolution. Through this approach, we achieved a very high effective revisit time of 1.93 days, equating to more than one observation every 2 days, which marks a significant advancement in temporal resolution over previous studies. For example, Gallart et al. (2016) were able to establish the duration of the hydrological conditions (or aquatic states) in 12 NPRs only on a monthly or seasonal scale. Maswanganye et al. (2024), using Sentinel-1 and S2 imagery, achieved a 10-day revisit time for two NPRs in South Africa. Similarly, Cavallo et al. (2022) reported a revisit time of 15 days when relying solely on S2 imagery for ungauged NPRs in Southern Italy. In their study, daily-scale assessments were then made possible by developing predictive models to estimate hydrological conditions between image acquisitions. In contrast, this study eliminated the need for such modeling by leveraging the high observational frequency enabled by the integration of S2 and PS imagery, which provided an average revisit time up to 1.5 days during summer 2022. This greatly simplifies and accelerates the characterization of hydrological regimes, a particularly valuable outcome especially for entirely ungauged NPR systems.

Our use of satellite imagery enabled a detailed characterization of the hydrological regime in the lower Sangone River, which is subject to flow intermittency caused by water abstractions. This approach identified drought periods and allowed us to quantify the relative frequency and duration of different hydrological conditions. Through our analysis, summer 2022 was identified as the most severe drought period, aligning with recent findings by Bonaldo et al. (2023), who reported 2022 as a year of prolonged drought across Northern Italy. In contrast, locally recorded hydrological data from the gauging station and the observation well, when considered alone, were insufficient for accurately assessing the frequency and duration of hydrological conditions within the monitored reach (Figure 5). Consistently with findings from Cavallo et al. (2022), the significant overlap between observed hydrological conditions and discharge or groundwater level data made simple correlations unfeasible (Figure S5 in Supporting Information S1). Even when the analysis was simplified to a binary classification (F and NF), it was not possible to identify a threshold that consistently distinguished these phases over the entire monitoring period (Figure S6 in Supporting Information S1). The limitations of using these data sources for describing the complex spatio-temporal dynamics of hydrological conditions in NPRs have already been pointed out by several authors (e.g., Bonada et al., 2020; Gallart et al., 2017; Zimmer et al., 2020). In our study, we observed the same inherent constraints, which were further exacerbated due to the water abstraction practices that affect the monitored reach. Particularly, groundwater level data showed weaker correlations with hydrological conditions, as the same levels corresponded to varying conditions (F, P, or D, Figure S5 in Supporting Information S1). Such complexities, also reported by Scanlon et al. (2002) and Sophocleous (2002), arise from the non-linear and variable relationships between groundwater levels and streamflow, influenced by several factors like rainfall intensity, soil characteristics, and land use. While in situ monitoring tools alone are often inadequate for capturing the complexity of NPRs hydrology, their integration with satellite-based observations provides a powerful means to characterize hydrological regimes. In this study, this combined approach enabled a detailed reconstruction of the P condition dynamics over the 7-year monitoring period (2017–2023). Specifically, we were able to determine the duration of multiple P events, revealing substantial variability in the transition from F to D

19447973, 2026, 3, Downloaded from https://agupubs.onlinelibrary.wiley.com/doi/10.1029/2025WR041133 by Politecnico Di Torino Sist. Bibl Del Polit Di Torino, Wiley Online Library on [07/10/2026]. See the Terms and Conditions (https://onlinelibrary.wiley.com/terms-and-conditions) on Wiley Online Library for rules of use; OA articles are governed by the applicable Creative Commons License

19447973, 2026, 3, Downloaded from https://agupubs.onlinelibrary.wiley.com/doi/10.1029/2025WR041133 by Politecnico Di Torino Sist. Bibl Del Polit Di Torino, Wiley Online Library on [07/10/2026]. See the Terms and Conditions (https://onlinelibrary.wiley.com/terms-and-conditions) on Wiley Online Library for rules of use; OA articles are governed by the applicable Creative Commons License

conditions (Figure 5). These transitions ranged from as short as 4 days (late August 2022) to as long as 96 days (summer 2017), demonstrating the importance of high-frequency monitoring.

The threshold discharge (Q^*) of 1.12 m^3/s in the Trana time series was used as a benchmark to identify when continuous flow ceased in the monitored reach during the most severe drought period corresponding to summer 2022 (Figure 6). Although the use of a fixed threshold may be considered a rough approximation (e.g., Yu et al., 2024), our analysis, focused on a critical period, demonstrated strong alignment with the satellite-derived hydrological conditions. Specifically, we achieved a Youden Index of 0.98 when the analysis was reduced to a binary classification problem (F and NF), and an overall classification accuracy of 85.1% across the three conditions (F, P, and D), both of which are notably high. The primary source of misclassification occurred in late September, when nine observed P conditions were interpreted as dry by the model. In our opinion, this discrepancy may be linked to changes in the water abstraction regime, which likely increased flow releases at the end of the irrigation season, particularly given the absence of any evident increase in streamflow or groundwater levels recorded in the study area (Figure 6b). Nevertheless, from an aquatic habitat perspective, this misclassification represents a conservative estimate. Moreover, the selected Q^* closely corresponds to the total licensed water abstraction (above 1 m^3/s) for the area, based on the available data from the Metropolitan City of Turin WebGIS. These results therefore support the suitability of this approach for characterizing the altered flow regime during the selected critical period (1 June–8 October). While this method was tested over a single timeframe, its extension to other periods appears feasible. In particular, as suggested by the analysis based on ROC curves, discharge thresholds could be defined and calibrated for each summer period to account for interannual variability in water availability. This perspective offers valuable insights for enhancing water resource management in the Sangone catchment. By integrating continuous discharge and groundwater level data from in situ monitoring stations with remotely sensed observations, it would be possible to dynamically establish zero-flow thresholds for downstream reaches during crop irrigation seasons, thereby enabling almost real-time drought mitigation and more effective resource planning.

However, constraints remain regarding the broader application of this methodology to different NPR reaches, particularly in estimating precise P durations from remotely sensed data. Despite S2 and PS currently providing the best trad off between GSD and revisit time among multispectral missions with global coverage, they still present inherent limitations related to both sensor characteristics and scene-dependent factors (e.g., cloud cover, shadows). Their effective spatial resolution (10 m for S2 and 3 m for PS) requires monitored reaches to have a minimum active channel width to ensure reliable detection of hydrological conditions. Previous studies suggest that at least three pixels are necessary for robust supervised classification (e.g., Cavallo et al., 2022; Jiang et al., 2014). The temporal dimension also poses challenges. Indeed, sufficient satellite coverage has only been available since 2017, precluding long-term analysis. Additionally, for NPRs with P durations near or below the effective revisit time (e.g., $\leq$1 day), overestimations may occur, leading to potentially incorrect habitat evaluations. In our case study on the Sangone River, several conditions supported the feasibility of the approach. The active channel width of the monitored reach ($\sim$42 m) exceeded the minimum threshold imposed by the S2 GSD, and the integration of PS data with a finer spatial resolution further improved water detection. This enhancement not only increased classification accuracy but also suggests the potential applicability of the method to narrower NPR reaches (i.e., $\sim$10–30 m in width), an aspect warranting further investigation. Furthermore, the monitored reach lies in a plain, away from steep terrain, and the presence of dense riparian vegetation is limited by intensive agricultural practices along its banks. These favorable conditions reduced the likelihood of shadowing, which could prevent water identification or lead to misclassifications. Regarding the temporal dimension, most of P conditions in the monitored reach (85% of total P) had durations exceeding 7 days, significantly longer than the effective revisit time we achieved. Additionally, NF phases predominantly occurred in summer, when cloud cover in Italy is generally minimal, thereby further improving the effective revisit time. Finally, the typical acquisition time of S2 and PS scenes over the study area ($\sim$09:30–10:30 a.m.) provided favorable illumination conditions, as the sun was already sufficiently high to minimize shadows, especially during summer.

Nevertheless, additional sources of uncertainty affecting the accuracy of our approach are linked to the reliance on supervised classification of satellite imagery. As extensively discussed by Cavallo et al. (2022) for S2 imagery, detecting water is not always possible. Small wetted areas ($\leq$10 m), depending on their relative position to image pixels, may fall below the detection capability, resulting in misclassification of hydrological conditions. This limitation is particularly critical during transitions from F to NF phases, when narrow wetted channels may still sustain flow continuity, or when residual ponds are too small to be captured, leading to confusion between P and D

19447973, 2026, 3, Downloaded from https://agupubs.onlinelibrary.wiley.com/doi/10.1029/2025WR041133 by Politecnico Di Torino Sist. Bibl Del Polit Di Torino, Wiley Online Library on [07/10/2026]. See the Terms and Conditions (https://onlinelibrary.wiley.com/terms-and-conditions) on Wiley Online Library for rules of use; OA articles are governed by the applicable Creative Commons License

conditions. Since the primary objective of the analysis was to estimate the duration of aquatic habitat availability, we applied a conservative rule: in cases of uncertainty, the worst hydrological condition was assigned (i.e., P for ambiguous F/FN cases, and D for ambiguous P/D cases). However, to mitigate classification errors, a three-step validation procedure was implemented. First, 12 HRIs available during the monitoring period were used as ground truth to validate our classification, with hydrological conditions derived from S2 and PS imagery perfectly matching those observed in the corresponding HRIs. Second, four independent field surveys conducted in the summers of 2021 and 2022 confirmed classification reliability during NF periods, again showing perfect correspondence. Third, to further assess consistency, we compared all same-day acquisitions from S2 and PS constellations (403 paired images in total) in a GIS environment. In every case, hydrological conditions were identically assigned, supporting a high level of robustness in the classification approach. Nonetheless, further measures can be adopted to reduce uncertainty. For example, Cavallo et al. (2022) validated supervised classifications of NPRs flow regime in Southern Italy using geolocated ground photos collected in the field during satellite overpasses. Maswanganye et al. (2024) enriched the classification of flow intermittency in South Africa NPRs by integrating Sentinel-1 radar data, while Hinrich Kaplan et al. (2019) employed strategically placed cameras to characterize flow regimes in small streams in Luxembourg. In our case, in addition to satellite data, locally recorded discharge and groundwater level time series were available. Although a complete hydrological picture of the monitored reach could not be reconstructed due to missing water abstraction data, these time series provided an independent data set for evaluating the accuracy of our classification. Specifically, by reducing the analysis to a binary classification problem (F vs. NF) and applying ROC curve analysis, we obtained an overall AUC $\geq$ 0.90 considering both discharge and groundwater level data, providing strong evidence of classification reliability during periods largely characterized by flow intermittency (i.e., summer). It is also important to emphasize that our reliance on a supervised approach, despite the limitations, was largely motivated by the current lack of transferable algorithms that can be consistently applied across different river systems and extended monitoring periods (Cavallo et al., 2022). To date, only a few methods have been specifically developed to distinguish water from non-water pixels in multispectral satellite images of NPRs. For example, Cavallo et al. (2025) proposed an algorithm for S2, while Wang and Vivoni (2022) introduced one for PS. Both studies, however, were restricted to specific NPRs systems and reported overall accuracies between 0.8 and 0.9 in detecting water presence, which may be considered comparable to the results achieved in our study.

4.2. Habitat Assessment

Meso-scale habitat simulation models (e.g., MesoHABSIM) have been widely used in the context of water resources planning and the management of perennial rivers (Yi et al., 2017). In Mediterranean watersheds, they have been successfully employed for defining mesohabitat requirements of different autochthonous freshwater species (Costarrosa et al., 2022; Negro et al., 2025; Pinna et al., 2024; Vezza et al., 2016). However, applications in NPRs have only recently gained momentum, reflecting an increased scientific interest in these dynamic environments (Blackman et al., 2021; Busch et al., 2020). For instance, Acuña et al. (2020) emphasized the potential of meso-scale habitat suitability models for evaluating aquatic habitats in NPRs using fish species as ecological indicators. Our study further supports this perspective, particularly through the innovative NPRs-module of SimStream-Web, which proved effective in assessing habitat dynamics during both F and NF phases for both fish and macroinvertebrate communities. Results from the Sangone River demonstrate the module's adaptability in evaluating aquatic habitats at different hydrological conditions and its potential for broader applications in NPR systems. These findings align with Negro et al. (2019), who started testing this module to account for habitat variability during NF phases in a highly regulated NPR in Catalonia (NE Spain).

The integration of proximal sensing and hydrodynamic modeling for aquatic habitat assessment is rapidly expanding, particularly for meso-scale analyses (Farò et al., 2025). To the best of our knowledge, this study represents the first attempt to quantify habitat availability for different freshwater communities in a non-perennial river using such an integrated framework. Regarding the bathymetric correction of the DEM, applied to mitigate optical refraction distortions in UAS-derived data, this study employed a simplified approach based on a linear regression model derived from Snell's law (slope = 1.33). Although site-specific calibration of such models is generally recommended (Negro et al., 2025), this simplified correction was deemed appropriate given the limited number of available ground control points and, in particular, the shallow water conditions characterizing the surveyed sub-reach during the UAS flight (mean depth = 0.07 m; maximum = 0.38 m). Indeed, the magnitude of bathymetric underestimation typically increases proportionally with water depth (Westaway et al., 2000);

19447973, 2026, 3, Downloaded from https://agupubs.onlinelibrary.wiley.com/doi/10.1029/2025WR041133 by Politecnico Di Torino Sist. Bibl Del Polit Di Torino, Wiley Online Library on [07/10/2026]. See the Terms and Conditions (https://onlinelibrary.wiley.com/terms-and-conditions) on Wiley Online Library for rules of use; OA articles are governed by the applicable Creative Commons License

therefore, under the conditions observed during the UAS flight, the potential error is expected to be minimal, approximately equivalent to the DEM spatial resolution (5.4 cm) and well below the most representative substrate size (mesolithal, 6–20 cm). This interpretation is consistent with previous findings indicating that, under shallow water conditions (<0.2 m), refraction correction is often unnecessary, as the mean vertical error is comparable to that observed over emerged terrain (Westaway et al., 2001). Moreover, slope values reported in literature for mono-parametric linear correction models (e.g., 1.5–1.6; Negro et al., 2025; Yudha Partama et al., 2017) would not have significantly increased the reprojection of the submerged riverbed under the shallow conditions observed during the UAS survey. Therefore, despite the absence of site-specific calibration, the corrected DEM can be considered reliable and well-suited for the hydraulic and habitat modeling objectives of this study. In developing the hydrodynamic model, particular attention was given to selecting an appropriate (a) mesh resolution and (b) bed roughness coefficient. Following established recommendations (Célik et al., 2008; Tonina & Jorde, 2013), a grid convergence analysis was performed, leading to the selection of a 0.25 m^2 mesh. This resolution is finer than those typically adopted in similar studies (~1 m^2) and is generally considered mesh-independent for habitat availability assessments in both micro- and meso-scale analyses (e.g., Farò et al., 2023; Papaioannou et al., 2020; Pasternack et al., 2004). Our tests confirmed this, showing habitat variation below 0.7% across the three considered grid configurations. Model calibration was conducted by adjusting the Manning's coefficient to minimize discrepancies between simulated and observed WSE, achieving a very high degree of correspondence (RMSE = 0.035 m). Although exhaustive validation (Tonina & Jorde, 2013) was not feasible due to the limited number of in situ depth and velocity measurements, the best-fitting Manning's value ($n = 0.045$) closely matched that predicted by the empirical relationship of Loukas and Quick (1996) based on reach slope. Moreover, in accordance with Tonina and Jorde (2013), the sensitivity analyses performed over the range of Manning's values (0.040–0.050) revealed negligible variations in fish habitat availability, with the maximum difference in the Flow-T index being less than 0.8%. Similarly, assigning spatially variable roughness values to substrate patches derived from the RGB orthomosaic produced no significant change in habitat availability across ecological targets. These results collectively indicate that the developed hydrodynamic model can be considered reliable and adequate for supporting the assessment of aquatic habitat availability in the monitored NPR reach.

Within the surveyed sub-reach, the hydrodynamic results revealed that water depths remained shallow (<0.70 m) across flow conditions, while flow velocities slightly increased with higher simulated discharges. The observed steep rise in wetted area with increasing discharge highlights the geomorphic influence of the low-confined, wide channel morphology, which promotes lateral inundation without significant increases in water depth. Substrate analysis indicated dominance by coarse grain sizes (mesolithal and macrolithal), resulting in a high distribution of boulders as cover attributes. These findings seem to further confirm the choice of a relatively high Manning's coefficient (i.e., 0.045) as bed roughness of the hydrodynamic model (Chow, 1988). Electrofishing surveys highlighted the ecological importance of the reach, identifying a significant presence of freshwater fish species. These findings align with recent literature on the biodiversity of NPRs, which recognizes such systems as important spots of freshwater species richness (e.g., Acuña et al., 2020; Skoulikidis et al., 2017).

The habitat availability for *T. muticellus*, assessed through the HSC included in SimStream-Web, revealed that adults preferred moderate flow conditions (>1.00 m^3/s), while juveniles favored lower flows (0.15 m^3/s, Figure 6a). These observations are consistent with their size-dependent flow preferences and are supported by (a) electrofishing data, which identified juveniles as the dominant life stage within the study area, and (b) previous findings reported in available literature (Harby et al., 2007; Negro et al., 2021). Conversely, habitat availability for adult *P. bonelli* was consistently higher, particularly at lower flow conditions. These results align with earlier studies that report a species' preference for shallow waters with low velocities (Vezza et al., 2012) and coarse substrates (Lugli et al., 1992; Negro et al., 2021), both of which are abundant in the study site. The Flow-T index during the F phase showed a consistent increase with discharge, reaching the maximum value (0.5) at the highest considered flow condition. This trend, consistent with the findings of Pinna et al. (2024), is due to the index's strong correlation with current velocity (Laini et al., 2022), which scales with discharge in this reach. During P conditions, isolated ponds still provided residual habitat for juvenile *T. muticellus*, adult *P. bonelli*, and macroinvertebrates until the reach transitioned to a completely D condition. Whereas adult *T. muticellus* was the most sensitive to flow cessation, with nearly no available habitat during the NF phase (~0.0 m^2). These results align with findings by Hodges and Magoulick (2011), who demonstrated that the effects of flow interruption on fish are species-specific. Notably, benthic organisms demonstrated the highest resilience, maintaining suitable habitat even under zero-flow conditions. These findings corroborate studies highlighting that isolated ponds serve as

19447973, 2026, 3, Downloaded from https://agupubs.onlinelibrary.wiley.com/doi/10.1029/2025WR041133 by Politecnico Di Torino Sist. Bibl Del Polit Di Torino, Wiley Online Library on [07/10/2026]. See the Terms and Conditions (https://onlinelibrary.wiley.com/terms-and-conditions) on Wiley Online Library for rules of use; OA articles are governed by the applicable Creative Commons License

critical refugia for sustaining aquatic communities during zero-flow events (e.g., Bonada et al., 2020; Kerezsy et al., 2017). Nonetheless, to preserve these species, it is crucial to maintain adequate surface flow regimes to minimize the duration of NF periods, thus avoiding completely D conditions. Our analysis indicates that during low-flow periods and heightened water withdrawals, NF phases should be interrupted with flow releases (sensu e-flows) at least every 8 days, on average, to prevent the complete loss of wetted area in the monitored reach. This flow release frequency would also help sustain suitable conditions in isolated pools during extended P phases, mitigating stressors such as elevated water temperatures and reduced dissolved oxygen.

Implementing the NPRs-module requires additional efforts compared to the standard MesoHABSIM approach used for perennial rivers, in order to characterize local physical habitat during NF periods. Specifically, surveys conducted during the P condition are important to describe aquatic habitat evolution after flow cessation. Moreover, it is critical to determine if and when the considered river reach moves to a completely D condition. To this end, further field surveys were planned in the study site during the summers of 2021 and 2022 to assess habitat availability during zero-flow periods, prior to reaching a completely D condition. However, these attempts did not allow for capturing the P condition due to rapid hydrological transitions (Figure 5) and the unpredictable impacts of water diversions, which introduce further variability in the transition from F to D conditions. Given these limitations, an alternative method was used to estimate residual aquatic habitat during the NF period. This involved artificially filling the bathymetrically corrected DEM in a GIS environment to simulate pond formation in the most depressed areas of the reach, where residual habitat is likely to persist during zero-flow periods. Although this method does not yield exact wetted area estimates, we implemented a two-step validation procedure that showed satisfactory agreement. First, according to what suggested by Yu et al. (2022), we verified the expected linear decline in wetted area prior to complete drying by analyzing wetted area extents using FCIs. Second, we qualitatively validated the modeled wetted areas on the first day after flow cessation using PS imagery classified as P during the summers of 2021 and 2022. This approach, combining high-resolution DEMs, satellite imagery, and georeferenced habitat attributes, proves to be a practical solution for rapidly estimating aquatic habitat at the meso-scale in NPRs during P conditions.

Information on P duration, derived from satellite image analysis, played a crucial role in defining habitat-flow-time rating curves for the monitored reach, as required by the innovative NPRs-module of the MesoHABSIM approach (Figure 6a). In this study, to evaluate aquatic habitat evolution during the NF phase, from the full range of observed P durations preceding dry out over the monitored period (from 4 to 96 days) we adopted the median value (i.e., 8 days) as a representative indicator of typical P persistence in the monitored reach. This assumption is supported by local hydro-morphological characteristics, as ponded mesohabitats remain environmentally suitable throughout this relatively short period despite hydraulic disconnection. Specifically, ponds are generally sustained by hyporheic fluxes through coarse, highly permeable riverbed sediments, which promote water renewal. This subsurface exchange provides thermal buffering, preventing water temperatures from exceeding known tolerance limits for the target species during the analyzed periods. Moreover, dissolved oxygen concentrations are expected to remain sufficiently high, given the limited organic pollution affecting the monitored reach and the short assumed ponding duration, which does not favor substantial algal biomass development or oxygen depletion. Nevertheless, alternative assumptions may be adopted to account for site-specific hydro-morphological conditions or species-specific ecological thresholds (e.g., fish thermal limit). In this regards, SimStream-Web offers the flexibility to explore different scenarios. For instance, users can analyze varying P durations (such as minimum or maximum durations over a selected period), enabling the computation of alternative habitat-flow-time rating curves. This allows the assessment of critical scenarios in aquatic habitat availability and the evaluation of alternative e-flow release strategies aimed at sustaining ecological integrity in the analyzed reaches.

Due to increasing anthropogenic pressures and climate change patterns, intermittency in watercourses is globally increasing (McDonough et al., 2011). Rivers that normally present a perennial behavior are changing their nature, assuming intermittent features along their course (Datry et al., 2014). This situation is particularly evident in the Sangone River, where current water abstraction licensing poses a significant threat to the survival of the aquatic ecosystem in its downstream reaches. An overall increase in the duration and frequency of zero-flow periods in different reaches below the village of Trana is observable in recent years, particularly during the summer months (July–September). To mitigate this situation, ecological flows (e-flows) must be defined and implemented, taking into account the frequency and duration of the P and the D conditions. In this context, the innovative NPRs-module of SimStream-Web emerges as a valuable tool for enhancing water resource management. By quantifying the habitat for aquatic organisms over flows and time after flow cessation, this module enables the analysis

19447973, 2026, 3, Downloaded from https://agupubs.onlinelibrary.wiley.com/doi/10.1029/2025WR041133 by Politecnico Di Torino Sist. Bibl Del Polit Di Torino, Wiley Online Library on [07/10/2026]. See the Terms and Conditions (https://onlinelibrary.wiley.com/terms-and-conditions) on Wiley Online Library for rules of use; OA articles are governed by the applicable Creative Commons License

of the deviation between natural and altered habitat time series. Consequently, different e-flows scenarios can be tested and evaluated to minimize the environmental impacts of water abstractions during low flow and drought periods, enhancing freshwater ecosystems and conserving local biodiversity. Beyond the Sangone River, the methodological framework developed in this study can be extended to NPRs of diverse climatic regions. Our approach, integrating (a) globally available satellite data, (b) hydrological assessments capable of defining local streamflow even with limited in situ records, and (c) the MesoHABSIM methodology, which relies on a detailed hydro-morphological characterization of aquatic habitat, provides a transferable tool to support e-flow implementation in NPRs worldwide. Its successful application, however, requires the fulfillment of several key conditions. First, the hydro-morphological context must be suitable, including sufficient channel width relative to the spatial resolution of satellite imagery, favorable terrain and riparian settings to minimize shadowing, and ponding durations that exceed the effective satellite revisit time to ensure reliable detection of hydrological conditions. Second, streamflow information, whether recorded or modeled, is essential to complement remotely sensed observations and enable accurate e-flow assessment. Third, ground-based observations are needed to validate satellite-based classifications across a range of hydrological conditions, ensuring reliable identification of ponding and dry phases. Finally, robust habitat suitability criteria must be available or specifically developed for the target community, which can be informed through targeted field sampling.

5. Conclusions

Preserving non-perennial rivers and streams and their ecosystems requires effective tools to describe the complex dynamics of aquatic habitats during both flowing and non-flowing phases. In this study, we utilized satellite data to characterize the hydrological regime of the Sangone River, a small regulated stream in Northern Italy, and integrated this information into the innovative NPRs-module of the MesoHABSIM approach. This integration allowed us to analyze fish and macroinvertebrate habitat availability as a function of flow and the time elapsed since flow cessation.

The study demonstrated the effectiveness of combining S2 and PS imagery for monitoring NPR hydrological regimes at an unprecedented temporal (1.93-day revisit time) resolution. Using a supervised classification approach, we identified F, P, and D conditions over a 7-year monitoring period (2017–2023). Results revealed significant variability in P durations (4–96 days) and identified severe drought periods, such as summer 2022, with up to 40 consecutive days of D riverbed.

The NPRs-module of SimStream-Web emerged as a powerful tool, seamlessly integrating remotely sensed and in situ hydrological data with high spatial and field-collected information to generate habitat-flow-time rating curves. These curves enabled analyzing aquatic habitat dynamics across flowing and non-flowing phases, providing a comprehensive understanding of the effects of altered flow regime on freshwater ecosystems. This methodology offers actionable insights for minimizing ecological impacts during droughts and low-flow periods.

Our study highlights the potential of the NPRs-module for water resource management for the intermittent stream network. By providing detailed insights into hydrological conditions and habitat availability, it supports the development of e-flows strategies. These strategies can mitigate the impacts of increasing flow intermittency caused by climate change and anthropogenic pressures, promoting the conservation of aquatic ecosystems in the Sangone River and similar systems worldwide.

Conflict of Interest

The authors declare no conflicts of interest relevant to this study.

Data Availability Statement

The results of the satellite based hydrological classification (2017–2023), along with the associated hydrological data sets (streamflow and groundwater level time series) are provided in Table S1. The streamflow time series recorded by the Environmental Protection Agency of the Piemonte Region is publicly accessible at https://www.arpa.piemonte.it/rischi_naturali/snippets_arpa_graphs/map_meteoweb/?rete=stazione_idrologica. The groundwater time series recorded by the Metropolitan City of Turin is publicly accessible at http://www.cittametropolitana.torino.it/cms/ambiente/risorse-idriche/progetti-ris-idriche/rete-monitoraggio/acque-sotterranee. Sentinel-2

satellite imagery is openly accessible through various platforms, including the Copernicus Data Space Browser: https://browser.dataspace.copernicus.eu/. The GIS data used to produce Figures 1 and 2, the code for generating Figures 5 and 6, and Figures S5 and S6 in Supporting Information S1, as well as the input and the output files for the aquatic habitat assessments performed using SimStream-Web, along with additional analysis results can be accessed from Zenodo repository: https://doi.org/10.5281/zenodo.15489770; (Negro et al., 2025). The SimStream-Web tool (Version 1.1.0), used for aquatic habitat assessments, is available under the GNU General Public License v3.0. It is hosted at: https://mesohabsim.isprambiente.it/app/home/, and was developed at the Polytechnic of Turin (Department of Environment, Land and Infrastructure Engineering—DIATI).

Acknowledgments
This research has been supported by the RIVERTEMP Erasmus+ project—Education for the identification and classification of temporary rivers to fight climate change (Grant 2022-1-IT02-KA220-HED-000086223), and by the Po River Basin Authority (Fondo per lo Sviluppo e la Coesione (FSC) 2014–2020—Piano Operativo Ambiente—Interventi per la Tutela del Territorio e delle Acque—Implementazione dei deflussi ecologici nei corsi d'acqua del distretto idrografico del fiume Po). Open access publishing facilitated by Politecnico di Torino, as part of the Wiley - CRUI-CARE agreement.

References

Acuña, V., Jorda-Capdevila, D., Vezza, P., De Girolamo, A. M., McClain, M. E., Stubbington, R., et al. (2020). Accounting for flow intermittency in environmental flows design. *Journal of Applied Ecology*, *57*(4), 742–753. https://doi.org/10.1111/1365-2664.13590

Anna, A., Yorgos, C., Konstantinos, P., & Maria, L. (2009). Do intermittent and ephemeral Mediterranean Rivers belong to the same river type? *Aquatic Ecology*, *43*(2), 465–476. https://doi.org/10.1007/s10452-008-9176-9

Arthington, A. H., Bernardo, J. M., & Ilhéu, M. (2014). Temporary rivers: Linking ecohydrology, ecological quality and reconciliation ecology. *River Research and Applications*, *30*(10), 1209–1215. https://doi.org/10.1002/rra.2831

Azar, R., Villa, P., Stroppiana, D., Crema, A., Boschetti, M., & Brivio, P. A. (2016). Assessing in-season crop classification performance using satellite data: A test case in Northern Italy. *European Journal of Remote Sensing*, *49*(1), 361–380. https://doi.org/10.5721/EuJRS20164920

Badino, G., Forneris, G., Pascale, M., & Perosino, G. C. (2002). La fauna ittica della Provincia di Torino. *Rivista Piemontese di Storia Naturale*, *24*, 295–326.

Balzamo, S., & Martone, C. (2014). Metodi biologici per le acque superficiali interne. In *ISPRA-Manuali e Linee Guida 111/2014*.

Belletti, B., Rinaldi, M., Bussettini, M., Comiti, F., Gurnell, A. M., Mao, L., et al. (2017). Characterising physical habitats and fluvial hydromorphology: A new system for the survey and classification of river geomorphic units. *Geomorphology*, *283*, 143–157. https://doi.org/10.1016/j.geomorph.2017.01.032

Blackman, R. C., Altermatt, F., Foulquier, A., Lefébure, T., Gauthier, M., Bouchez, A., et al. (2021). Unlocking our understanding of intermittent rivers and ephemeral streams with genomic tools. *Frontiers in Ecology and the Environment*, *19*(10), 574–583. https://doi.org/10.1002/fee.2404

Bonada, N., Cañedo-Argüelles, M., Gallart, F., von Schiller, D., Fortuño, P., Latron, J., et al. (2020). Conservation and management of isolated pools in temporary rivers. *Water*, *12*(10), 1–24. https://doi.org/10.3390/w12102870

Bonaldo, D., Bellafiore, D., Ferrarin, C., Ferretti, R., Ricchi, A., Sangelantoni, L., & Vitelletti, M. L. (2023). The summer 2022 drought: A taste of future climate for the Po valley (Italy)? *Regional Environmental Change*, *23*(1), 1–6. https://doi.org/10.1007/s10113-022-02004-z

Bourke, S. A., Shanafield, M., Hedley, P., Chapman, S., & Dogramaci, S. (2021). A hydrological framework for persistent river pools. *Hydrology and Earth System Sciences Discussions*, *2021*, 1–50. https://doi.org/10.5194/HESS-2020-133

Bovee, K. D. (1982). A guide to stream habitat analysis using the instream incremental flow methodology. In *Instream flow information paper* (Vol. 12, No. (82). United States Fish and Wildlife Service. FWS/OBS-82/26.

Busch, M. H., Costigan, K. H., Fritz, K. M., Datry, T., Krabbenhoft, C. A., Hammond, J. C., et al. (2020). What's in a name? Patterns, trends, and suggestions for defining non-perennial rivers and streams. *Water*, *12*(7), 1980. https://doi.org/10.3390/w12071980

Bussettini, M., & Vezza, P. (2019). Guidance on environmental flows—Integrating e-flow science with fluvial geomorphology to maintain ecosystem services.

Cavallo, C., Papa, M. N., Negro, G., Gargiulo, M., Ruello, G., & Vezza, P. (2022). Exploiting Sentinel-2 dataset to assess flow intermittency in non-perennial rivers. *Scientific Reports*, *12*(1), 1–16. https://doi.org/10.1038/s41598-022-26034-z

Cavallo, C., Sarno, L., Papa, M. N., Negro, G., Vezza, P., Ruello, G., & Gargiulo, M. (2025). Estimating dry bed periods in non-perennial rivers using Sentinel-2 satellite data. *Journal of Hydrology*, *660*, 133416. https://doi.org/10.1016/j.jhydrol.2025.133416

Célik, I. B., Ghia, U., Roache, P. J., & Freitas, C. J. (2008). Procedure for estimation and reporting of uncertainty due to discretization in CFD applications. *Journal of fluids Engineering-Transactions of the ASME*, *130*(7). https://doi.org/10.1115/1.2960953

Chow, V. T. (1988). *Open-channel hydraulics, classical textbook reissue*. MC Graw Hill Seattle.

Costarrosa, A., Jorda-Capdevila, D., Porcar, A., López-Doval, J. C., Pou-Rovira, Q., Herrero, A., et al. (2022). Suitability models at mesohabitat scale of native freshwater fish and mussels for their application. In *Environmental flows assessment in the NE of the Iberian Peninsula* (Vol. 138). https://doi.org/10.3390/blsf2022013138

Datry, T., Larned, S. T., & Tockner, K. (2014). Intermittent rivers: A challenge for freshwater ecology. *BioScience*, *64*(3), 229–235. https://doi.org/10.1093/BIOSCI/BIT027

Datry, T., Singer, G., Sauquet, E., Jorda-Capdevila, D., Von Schiller, D., Stubbington, R., et al. (2017). Science and management of intermittent rivers and ephemeral streams (SMIRES). *Research Ideas and Outcomes*, *3*, e21774. https://doi.org/10.3897/rio.3.e21774

Dietrich, J. T. (2017). Bathymetric structure-from-motion: Extracting shallow stream bathymetry from multi-view stereo photogrammetry. *Earth Surface Processes and Landforms*, *42*(2), 355–364. https://doi.org/10.1002/esp.4060

Döll, P., & Schmied, H. M. (2012). How is the impact of climate change on river flow regimes related to the impact on mean annual runoff? A global-scale analysis. *Environmental Research Letters*, *7*(1), 014037. https://doi.org/10.1088/1748-9326/7/1/014037

Dornes, P. F., & Comas, R. N. (2025). Hydrological regime index for non-perennial rivers. *Hydrology and Earth System Sciences*, *29*(13), 2901–2923. https://doi.org/10.5194/hess-29-2901-2025

European Union. (2000). Directive 2000/60/EC of the European Parliament and of the Council of 23 October 2000 establishing a framework for Community action in the field of water policy (Vol. *327*, pp. 1–73).

Farò, D., Baumgartner, K., Vezza, P., & Zolezzi, G. (2022). A novel unsupervised method for assessing mesoscale river habitat structure and suitability from 2D hydraulic models in gravel-bed rivers. *Ecohydrology*, *15*(7), 1–18. https://doi.org/10.1002/eco.2452

Farò, D., Baumgartner, K., Vezza, P., & Zolezzi, G. (2023). Sensitivity of fish habitat suitability to multi-resolution hydraulic modeling and field-based description of meso-scale river habitats. *Journal of Hydrology X*, *21*, 100160. https://doi.org/10.1016/j.hydroa.2023.100160

Farò, D., Soto Parra, T., Baumgartner, K., Andreoli, A., Vezza, P., & Zolezzi, G. (2025). An integrated framework for the assessment of meso-scale physical habitats in gravel-bed rivers using remote sensing and 2D hydraulic modeling. *Wiley Interdisciplinary Reviews: Water*, *12*(3), e70027. https://doi.org/10.1002/wat2.70027

19447973, 2026, 3, Downloaded from https://agupubs.onlinelibrary.wiley.com/doi/10.1029/2025WR041133 by Politecnico Di Torino Sist. Bibl Del Polit Di Torino, Wiley Online Library on [07/10/2026]. See the Terms and Conditions (https://onlinelibrary.wiley.com/terms-and-conditions) on Wiley Online Library for rules of use; OA articles are governed by the applicable Creative Commons License

Fluss, R., Faraggi, D., & Reiser, B. (2005). Estimation of the Youden Index and its associated cutoff point. *Biometrical Journal: Journal of Mathematical Methods in Biosciences*, *47*(4), 458–472. https://doi.org/10.1002/bimj.200410135

Frazier, A. E., & Hemingway, B. L. (2021). A technical review of planet smallsat data: Practical considerations for processing and using planetscope imagery. *Remote Sensing*, *13*(19), 3930. https://doi.org/10.3390/rs13193930

Gallart, F., Cid, N., Latron, J., Llorens, P., Bonada, N., Jeuffroy, J., et al. (2017). TREHS: An open-access software tool for investigating and evaluating temporary river regimes as a first step for their ecological status assessment. *Science of the Total Environment*, *607*, 519–540. https://doi.org/10.1016/j.scitotenv.2017.06.209

Gallart, F., Llorens, P., Latron, J., Cid, N., Rieradevall, M., & Prat, N. (2016). Validating alternative methodologies to estimate the regime of temporary rivers when flow data are unavailable. *Science of the Total Environment*, *565*, 1001–1010. https://doi.org/10.1016/j.scitotenv.2016.05.116

Gurnell, M., Bussettini, M., Camenen, B., González Del Tánago, M., Grabowski, R., Hendriks, D., et al. (2014). REstoring rivers FOR effective catchment Management (REFORM). In *Deliverable D2.1 Part I. A hierarchical multi-scale framework and indicators of hydromorphological processes and forms*.

Harby, A., Olivier, J. M., Merigoux, S., & Malet, E. (2007). A mesohabitat method used to assess minimum flow changes and impacts on the invertebrate and fish fauna in the Rhône River, France. *River Research and Applications*, *23*(5), 525–543. https://doi.org/10.1002/rra.997

Hinrich Kaplan, N., Sohrt, E., Blume, T., & Weiler, M. (2019). Monitoring ephemeral, intermittent and perennial streamflow: A dataset from 182 sites in the Attert catchment, Luxembourg. *Earth System Science Data*, *11*(3), 1363–1374. https://doi.org/10.5194/essd-11-1363-2019

Hodges, S. W., & Magoulick, D. D. (2011). Refuge habitats for fishes during seasonal drying in an intermittent stream: Movement, survival and abundance of three minnow species. *Aquatic Sciences*, *73*(4), 513–522. https://doi.org/10.1007/s00027-011-0206-7

Jiang, H., Feng, M., Zhu, Y., Lu, N., Huang, J., & Xiao, T. (2014). An automated method for extracting rivers and lakes from Landsat imagery. *Remote Sensing*, *6*(6), 5067–5089. https://doi.org/10.3390/rs6065067

Jorde, K. (1997). *Ökologisch begründete, dynamische Mindestwasserregelungen bei Ausleitungskraftwerken*. Eigenverlag des Instituts für Wasserbau der Universität.

Kemp, J. L., Harper, D. M., & Crosa, G. A. (1999). Use of "functional habitats" to link ecology with morphology and hydrology in river rehabilitation. *Aquatic Conservation: Marine and Freshwater Ecosystems*, *9*(1), 159–178. https://doi.org/10.1002/(SICI)1099-0755(199901/02)9:1<159::AID-AQC319>3.0.CO;2-M

Kerezsy, A., Gido, K., Magalhães, M. F., & Skelton, P. H. (2017). The biota of intermittent rivers and ephemeral streams: Fishes. In *Intermittent rivers and ephemeral streams*. Elsevier Inc. https://doi.org/10.1016/B978-0-12-803835-2.00010-3

Koutrakis, E. T., Triantafillidis, S., Sapounidis, A. S., Vezza, P., Kamidis, N., Sylaios, G., & Comoglio, C. (2019). Evaluation of ecological flows in highly regulated rivers using the mesohabitat approach: A case study on the Nestos River, N. Greece. *Ecohydrology and Hydrobiology*, *19*(4), 598–609. https://doi.org/10.1016/j.ecohyd.2018.01.002

Krabbenhoft, C. A., Allen, G. H., Lin, P., Godsey, S. E., Allen, D. C., Burrows, R. M., et al. (2022). Assessing placement bias of the global river gauge network. *Nature Sustainability*, *5*(7), 586–592. https://doi.org/10.1038/s41893-022-00873-0

Laini, A., Burgazzi, G., Chadd, R., England, J., Tziortzis, I., Ventrucci, M., et al. (2022). Using invertebrate functional traits to improve flow variability assessment within European rivers. *Science of the Total Environment*, *832*, 155047. https://doi.org/10.1016/j.scitotenv.2022.155047

Larned, S. T., Datry, T., Arscott, D. B., & Tockner, K. (2010). Emerging concepts in temporary-river ecology. *Freshwater Biology*, *55*(4), 717–738. https://doi.org/10.1111/j.1365-2427.2009.02322.x

Leone, M., Gentile, F., Lo Porto, A., Ricci, G. F., & De Girolamo, A. M. (2023). Ecological flow in southern Europe: Status and trends in non-perennial rivers. *Journal of Environmental Management*, *342*, 118097. https://doi.org/10.1016/j.jenvman.2023.118097

Leopold, L. B., Wolman, M. G., Miller, J. P., & Wohl, E. E. (1964). *Fluvial processes in geomorphology*. W. H. Freeman & Company.

Lingua, A. M., Maschio, P., Spadaro, A., Vezza, P., & Negro, G. (2023). Iterative refraction-correction method on MVS-SFM for shallow stream bathymetry. *The International Archives of the Photogrammetry, Remote Sensing and Spatial Information Sciences*, *48*, 249–255. https://doi.org/10.5194/isprs-archives-xlviii-1-w1-2023-249-2023

Llanos-Paez, O., & Acuña, V. (2022). Analysis of the socio-ecological drivers of the recreational use of temporary streams and rivers. *Science of the Total Environment*, *807*, 150805. https://doi.org/10.1016/j.scitotenv.2021.150805

Loukas, A., & Quick, M. C. (1996). Physically-based estimation of lag time for forested mountainous watersheds. *Hydrological Sciences Journal*, *41*(1), 1–19. https://doi.org/10.1080/02626669609491475

Lugli, M., Bobbio, L., Torricelli, P., & Gandolfi, G. (1992). Breeding ecology and male spawning success in two hill-stream populations of the freshwater goby, *Padogobius martensi*. *Environmental Biology of Fishes*, *35*(1), 37–48. https://doi.org/10.1007/BF00001156

Magand, C., Helena Alves, M., Calleja, E., Datry, T., Dörflinger, G., & England, J. (2020). Intermittent rivers and ephemeral streams: What water managers need to know. https://doi.org/10.5281/zenodo.3888474

Maswanganye, S. E., Dube, T., Jovanovic, N., Kapangaziwiri, E., & Mazvimavi, D. (2024). Assessment of the spatiotemporal dynamics of the hydrological state of non-perennial river systems and identification of flow-contributing areas. *Water SA*, *50*(1), 32–44. https://doi.org/10.17159/wsa/2024.v50.i1.4046

Maswanganye, S. E., Dube, T., Mazvimavi, D., & Jovanovic, N. (2022). Remotely sensed applications in monitoring the spatio-temporal dynamics of pools and flows along non-perennial rivers: A review. *South African Geographical Journal*, *104*(4), 427–445. https://doi.org/10.1080/03736245.2021.1967774

McDonough, O. T., Hosen, J. D., & Palmer, M. A. (2011). Temporary streams: The hydrology, geography, and ecology of non-perennially flowing waters. In *River ecosystems: Dynamics, management and conservation* (pp. 259–290).

Messager, M. L., Lehner, B., Cockburn, C., Lamouroux, N., Pella, H., Snelder, T., et al. (2021). Global prevalence of non-perennial rivers and streams. *Nature*, *594*(7863), 391–397. https://doi.org/10.1038/s41586-021-03565-5

Munné, A., Bonada, N., Cid, N., Gallart, F., Solà, C., Bardina, M., et al. (2021). A proposal to classify and assess ecological status in Mediterranean temporary rivers: Research insights to solve management needs. *Water*, *13*(6), 767. https://doi.org/10.3390/w13060767

Murase, T., Tanaka, M., Tani, T., Miyashita, Y., Ohkawa, N., Ishiguro, S., et al. (2008). A photogrammetric correction procedure for light refraction effects at a two-medium boundary. *Photogrammetric Engineering & Remote Sensing*, *74*(9), 1129–1136. https://doi.org/10.14358/PERS.74.9.1129

Negro, G., Fenoglio, S., Quaranta, E., Comoglio, C., Garzia, I., & Vezza, P. (2021). Habitat preferences of Italian freshwater fish: A systematic review of data availability for applications of the MesoHABSIM model. *Frontiers in Environmental Science*, *9*, 305. https://doi.org/10.3389/fenvs.2021.634737

Negro, G., Lesa, D., Bertoli, M., Guglielmetto, A., Pinna, B., Forte, S., et al. (2025). Mesohabitat spawning preference of the Anadromous Twaite Shad (*Alosa fallax*, Lacépède 1803) in the Tagliamento River (Italy). *Ecohydrology*, *18*(1), e70010. https://doi.org/10.1002/eco.70010

19447973, 2026, 3, Downloaded from https://agupubs.onlinelibrary.wiley.com/doi/10.1029/2025WR041133 by Politecnico Di Torino Sist. Bibl Del Polit Di Torino, Wiley Online Library on [07/10/2026]. See the Terms and Conditions (https://onlinelibrary.wiley.com/terms-and-conditions) on Wiley Online Library for rules of use; OA articles are governed by the applicable Creative Commons License

Negro, G., Marino, A., Forte, S., Lo Conte, P., Bo, T., Fenoglio, S., & Vezza, P. (2023). Ecological notes on an endemic freshwater lamprey, *Lampetra zanandreai* (Vladykov, 1955). *European Zoological Journal*, *90*(2), 556–567. https://doi.org/10.1080/24750263.2023.2226680

Negro, G., Vezza, P., Jorda-Capdevila, D., Bardina, M., Garcia Burgos, E., Sola Ortega, C., & Munné, A. (2019). Meso-scale habitat modeling in temporary rivers: The Gaià River case study. In *Actas Del III Congreso Ibérico de Restauración Fluvial* (pp. 178–186).

Papaioannou, G., Papadaki, C., & Dimitriou, E. (2020). Sensitivity of habitat hydraulic model outputs to DTM and computational mesh resolution. *Ecohydrology*, *13*(2), e2182. https://doi.org/10.1002/eco.2182

Parasiewicz, P. (2007). The mesohabsim model revisited. *River Research and Applications*, *23*(8), 893–903. https://doi.org/10.1002/rra.1045

Parasiewicz, P., Rogers, J. N., Vezza, P., Gortázar, J., Seager, T., Pegg, M., et al. (2013). Applications of the MesoHABSIM simulation model. In *Ecohydraulics: An integrated approach* (pp. 109–124). John Wiley & Sons, Ltd. https://doi.org/10.1002/9781118526576.ch6

Parasiewicz, P., Ryan, K., Vezza, P., Comoglio, C., Ballestero, T., & Rogers, J. N. (2013). Use of quantitative habitat models for establishing performance metrics in river restoration planning. *Ecohydrology*, *6*(4), 668–678. https://doi.org/10.1002/eco.1350

Pasternack, G. B., Wang, C. L., & Merz, J. E. (2004). Application of a 2D hydrodynamic model to design of reach-scale spawning gravel replenishment on the Mokelumne River, California. *River Research and Applications*, *20*(2), 205–225. https://doi.org/10.1002/rra.748

Petts, G. E. (2009). Instream flow science for sustainable river management. *JAWRA Journal of the American Water Resources Association*, *45*(5), 1071–1086. https://doi.org/10.1111/J.1752-1688.2009.00360.X

Pinna, B., Laini, A., Negro, G., Burgazzi, G., Viaroli, P., & Vezza, P. (2024). Physical habitat modeling for river macroinvertebrate communities. *Journal of Environmental Management*, *358*, 120919. https://doi.org/10.1016/j.jenvman.2024.120919

Poff, N. L., Richter, B. D., Arthington, A. H., Bunn, S. E., Naiman, R. J., Kendy, E., et al. (2010). The ecological limits of hydrologic alteration (ELOHA): A new framework for developing regional environmental flow standards. *Freshwater Biology*, *55*(1), 147–170. https://doi.org/10.1111/j.1365-2427.2009.02204.x

Politecnico di Torino (DIATI). (2024). SimStream-Web (Version 1.1.0) [Software]. *Istituto Superiore per la Protezione e la Ricerca Ambientale (ISPRA)*. Retrieved from https://mesohabsim.isprambiente.it/app/home/

Pumo, D., Caracciolo, D., Viola, F., & Noto, L. V. (2016). Climate change effects on the hydrological regime of small non-perennial river basins. *Science of the Total Environment*, *542*, 76–92. https://doi.org/10.1016/J.SCITOTENV.2015.10.109

Roy, D. P., Huang, H., Houborg, R., & Martins, V. S. (2021). A global analysis of the temporal availability of PlanetScope high spatial resolution multi-spectral imagery. *Remote Sensing of Environment*, *264*, 112586. https://doi.org/10.1016/j.rse.2021.112586

Santato, S., Mysiak, J., & Pérez-Blanco, C. D. (2016). The water abstraction license regime in Italy: A case for reform? *Water*, *8*(3), 103. https://doi.org/10.3390/w8030103

Sauquet, E., Shanafield, M., Hammond, J. C., Sefton, C., Leigh, C., & Datry, T. (2021). Classification and trends in intermittent river flow regimes in Australia, northwestern Europe and USA: A global perspective. *Journal of Hydrology*, *597*, 126170. https://doi.org/10.1016/j.jhydrol.2021.126170

Scanlon, B. R., Healy, R. W., & Cook, P. G. (2002). Choosing appropriate techniques for quantifying groundwater recharge. *Hydrogeology Journal*, *10*(1), 18–39. https://doi.org/10.1007/s10040-001-0176-2

Seaman, M., Watson, M., Avenant, M., King, J., Joubert, A., Barker, C., et al. (2016). DRIFT-ARID: A method for assessing environmental water requirements (EWRs) for non-perennial rivers. *Water SA*, *42*(3), 356–367. https://doi.org/10.4314/wsa.v42i3.01

Skoulikidis, N. T., Sabater, S., Datry, T., Morais, M. M., Buffagni, A., Dörflinger, G., et al. (2017). Non-perennial Mediterranean rivers in Europe: Status, pressures, and challenges for research and management. *Science of the Total Environment*, *577*, 1–18. https://doi.org/10.1016/j.scitotenv.2016.10.147

Sophocleous, M. (2002). Interactions between groundwater and surface water: The state of the science. *Hydrogeology Journal*, *10*(1), 52–67. https://doi.org/10.1007/s10040-001-0170-8

Tayer, T. C., Beesley, L. S., Douglas, M. M., Bourke, S. A., Callow, J. N., Meredith, K., & McFarlane, D. (2023). Ecohydrological metrics derived from multispectral images to characterize surface water in an intermittent river. *Journal of Hydrology*, *617*, 129087. https://doi.org/10.1016/j.jhydrol.2023.129087

Tayer, T. C., Beesley, L. S., Douglas, M. M., Bourke, S. A., Meredith, K., & McFarlane, D. (2023). Identifying intermittent river sections with similar hydrology using remotely sensed metrics. *Journal of Hydrology*, *626*, 130266. https://doi.org/10.1016/j.jhydrol.2023.130266

Tennant, D. L. (1976). Instream flow regimens for fish, wildlife, recreation and related environmental resources. *Fisheries*, *1*(4), 6–10. https://doi.org/10.1577/1548-8446(1976)001<0006:IFRFFW>2.0.CO;2

Tewinkel, G. (1963). Water depths from aerial photographs. *Photogrammetric Engineering*, *29*(6), 1421–1428.

Tonina, D., & Jorde, K. (2013). Hydraulic modelling approaches for ecohydraulic studies: 3D, 2D, 1D and non-numerical models. In *Ecohydraulics: An integrated approach* (pp. 31–74). https://doi.org/10.1002/9781118526576.ch3

Tzoraki, O., & Nikolaidis, N. P. (2007). A generalized framework for modeling the hydrologic and biogeochemical response of a Mediterranean temporary river basin. *Journal of Hydrology*, *346*(3–4), 112–121. https://doi.org/10.1016/J.JHYDROL.2007.08.025

Vezza, P., Ghia, D., & Fea, G. (2016). Quantitative habitat models for the conservation of the endangered European crayfish *Austropotamobius pallipes* complex (Astacoidea: Astacidae). In *A global overview of the conservation of freshwater decapod crustaceans* (pp. 339–358). Springer International Publishing. https://doi.org/10.1007/978-3-319-42527-6_12

Vezza, P., Parasiewicz, P., Calles, O., Spairani, M., & Comoglio, C. (2014). Modelling habitat requirements of bullhead (*Cottus gobio*) in Alpine streams. *Aquatic Sciences*, *76*(1), 1–15. https://doi.org/10.1007/s00027-013-0306-7

Vezza, P., Parasiewicz, P., Rosso, M., & Comoglio, C. (2012). Defining minimum environmental flows at regional scale: Application of mesoscale habitat models and catchments classification. *River Research and Applications*, *28*(6), 717–730. https://doi.org/10.1002/rra.1571

Vezza, P., Parasiewicz, P., Spairani, M., & Comoglio, C. (2014). Habitat modeling in high-gradient streams: The mesoscale approach and application. *Ecological Applications*, *24*(4), 844–861. https://doi.org/10.1890/11-2066.1

Vezza, P., Zanin, A., & Parasiewicz, P. (2017). Manuale tecnico-operativo per la modellazione e la valutazione dell'integrità dell'habitat fluviale. In *ISPRA-Manuali e Linee Guida* (pp. 154–2017).

Wang, Z., & Vivoni, E. R. (2022). Detecting streamflow in dryland rivers using CubeSats. *Geophysical Research Letters*, *49*(15), 1–10. https://doi.org/10.1029/2022GL098729

Wegscheider, B., Linnansaari, T., & Curry, R. A. (2020). Mesohabitat modelling in fish ecology: A global synthesis. *Fish and Fisheries*, *21*(5), 927–939. https://doi.org/10.1111/faf.12477

Westaway, R. M., Lane, S. N., & Hicks, D. M. (2000). The development of an automated correction procedure for digital photogrammetry for the study of wide, shallow, gravel-bed rivers. *Earth Surface Processes and Landforms: The Journal of the British Geomorphological Research Group*, *25*(2), 209–226. https://doi.org/10.1002/(SICI)1096-9837(200002)25:2<209::AID-ESP84>3.0.CO;2-Z

Westaway, R. M., Lane, S. N., & Hicks, D. M. (2001). Remote sensing of clear-water, shallow, gravel-bed rivers using digital photogrammetry. *Photogrammetric Engineering & Remote Sensing*, *67*(11), 1271–1282.

19447973, 2026, 3, Downloaded from https://agupubs.onlinelibrary.wiley.com/doi/10.1029/2025WR041133 by Politecnico Di Torino Sist. Bibl Del Polit Di Torino, Wiley Online Library on [07/10/2026]. See the Terms and Conditions (https://onlinelibrary.wiley.com/terms-and-conditions) on Wiley Online Library for rules of use; OA articles are governed by the applicable Creative Commons License

Woodget, A. S., Carbonneau, P. E., Visser, F., & Maddock, I. P. (2015). Quantifying submerged fluvial topography using hyperspatial resolution UAS imagery and structure from motion photogrammetry. *Earth Surface Processes and Landforms*, *40*(1), 47–64. https://doi.org/10.1002/esp.3613

Wu, Q. (2020). geemap: A Python package for interactive mapping with Google Earth Engine. *Journal of Open Source Software*, *5*(51), 2305. https://doi.org/10.21105/joss.02305

Yeakley, J. A., Ervin, D., Chang, H., Granek, E. F., Dujon, V., Shandas, V., & Brown, D. (2016). Ecosystem services of streams and rivers. In *River science: Research and management for the 21st century* (pp. 335–352). John Wiley & Sons, Ltd. https://doi.org/10.1002/9781118643525.ch17

Yi, Y., Cheng, X., Yang, Z., Wieprecht, S., Zhang, S., & Wu, Y. (2017). Evaluating the ecological influence of hydraulic projects: A review of aquatic habitat suitability models. *Renewable and Sustainable Energy Reviews*, *68*, 748–762. https://doi.org/10.1016/j.rser.2016.09.138

Yu, S., Burrows, R. M., Shanafield, M., & Kennard, M. J. (2022). Water-level recession characteristics in isolated pools within non-perennial streams. *Advances in Water Resources*, *166*, 104267. https://doi.org/10.1016/j.advwatres.2022.104267

Yu, S., Shanafield, M., & Kennard, M. J. (2024). Assessing the influence of zero-flow threshold choice for characterising intermittent stream hydrology. *Hydrological Processes*, *38*(10), e15300. https://doi.org/10.1002/hyp.15300

Yudha Partama, I. G., Kanno, A., Akamatsu, Y., Inui, R., Goto, M., & Sekine, M. (2017). A simple and empirical refraction correction method for UAV-based shallow-water photogrammetry. *International Journal of Scholarly and Scientific Research & Innovation*, *11*(4), 254–261.

Zimmer, M. A., Kaiser, K. E., Blaszczak, J. R., Zipper, S. C., Hammond, J. C., Fritz, K. M., et al. (2020). Zero or not? Causes and consequences of zero-flow stream gage readings. *Wiley Interdisciplinary Reviews: Water*, *7*(3), e1436. https://doi.org/10.1002/wat2.1436

19447973, 2026, 3, Downloaded from https://agupubs.onlinelibrary.wiley.com/doi/10.1029/2025WR041133 by Politecnico Di Torino Sist. Bibl Del Polit Di Torino, Wiley Online Library on [07/10/2026]. See the Terms and Conditions (https://onlinelibrary.wiley.com/terms-and-conditions) on Wiley Online Library for rules of use; OA articles are governed by the applicable Creative Commons License